Morphology of Hippocampal Neurons

Imre Vida, Claudius E. Degro, and Sam A. Booker

Overview

"Form follows function" states the credo of modern architecture, defining how the shape of an object should be determined by its function. While natural objects, such as neurons, have not taken their shape from design boards, the inquisitive observer can nevertheless gain insights about their function by studying morphological features. This teleological mindset was the main driving force behind the early neuroanatomical investigations, which culminated in the work of Cajal and formed the foundation of modern neuroscience. Neuroanatomical analysis remains an essential part of neuroscience research today and computational neuroscientists particularly benefit from the flow of morphological data, with increasing detail and resolution.

Nerve cells or neurons are the structural and functional units of the nervous system and come in various sizes and shapes, conceivably reflecting differences in the functional roles played by them in brain circuits. On the one hand, the distribution of dendrites and axon determines the synaptic inputs and available targets to cells. On the other hand, the three-dimensional structure of neuronal processes constitutes the cable structure in which signals are integrated and processed.

Neurons in cortical areas, including the hippocampus, can be broadly divided into two major classes: principal cells and non-principal cells or interneurons. Principal cells comprise the majority (~80–90%) of the neuronal population with area-specific morphological features. While they are regarded largely homogeneous

I. Vida (✉) · C. E. Degro
Institute for Integrative Neuroanatomy, Charité – Universitätsmedizin Berlin, Berlin, Germany
e-mail: imre.vida@charite.de

S. A. Booker
Centre for Discovery Brain Sciences, University of Edinburgh, Edinburgh, UK

V. Cutsuridis et al. (eds.), *Hippocampal Microcircuits*, Springer Series
in Computational Neuroscience, https://doi.org/10.1007/978-3-319-99103-0_2

within an area, there is increasing evidence for position-dependent differences in their properties. Cortical principal cells are excitatory glutamatergic neurons and are considered to be the workhorse of information processing. They send axon collaterals to other brain areas and therefore are also referred to as "projection neurons." Interneurons are inhibitory, GABAergic, cells and are characterized by dense local axonal arbor which enables them to control and coordinate the activity of large populations of local neurons. Although interneurons comprise only a small proportion of the neuronal population (~10–20%), they display a high degree of morphological heterogeneity and can be subdivided into a number of types. The diversity of the interneurons conceivably serves a division of labor in spatiotemporal control of principal cell activity, much like a conductor leading an orchestra.

In this chapter we will review the morphological characteristics and local connectivity of the various neuron types in the hippocampus of rodents. Although due to the possibilities offered by genetically modified organisms and elegant optogenetic approaches, studies more commonly use mice nowadays, the majority of the cellular level data available in the literature are still from the rat hippocampus.

The Data

Anatomical Structure and Nomenclature

The hippocampus is a phylogenetically ancient cortical structure ("archicortex") which evolved from the dorsomedial aspects of the cerebral hemispheres. It consists of two interlocked folds of the cortical mantel, the hippocampus proper and the dentate gyrus (DG; Cajal 1968; Lorente de Nó 1934). Macroscopically the curved structure of the hippocampus bears some resemblance to the horns of a ram, hence the Latin *cornu ammonis* (CA). Its cranial ("septal") pole is located close to the midline in the dorsal part of the hemisphere, below the *corpus callosum*, whereas its caudal ("temporal") pole extends ventrolaterally into the temporal lobes (see Fig. 1 in the chapter "Connectivity of the Hippocampus").

In cross section, the hippocampus proper (CA areas) and the DG form two interlocked "C" shapes (Fig. 1). The hippocampus proper features pyramidal cells and can be cytoarchitecturally divided into the CA1, CA2, and CA3 areas. Lorente de Nó (1934) further subdivided the CA1 and CA3 areas to three zones along the transverse axis: "a" (closer to the subiculum), "b," and "c" (closer to the hilus) on the basis of their anatomical connectivity. In contrast to the CA regions, the DG comprises a population of granule cells (GC) as principal neurons. The interface between the DG and CA areas is called the *hilus* which contains a third population of principal cells, the mossy cells. The *hilus* differs from other parts of the hippocampus in that it shows no clear lamination, and the ratio of principal cells and interneurons is close to equal. It has been a matter of some controversy whether it belongs to the hippocampus proper as a CA4 area (Lorente de Nó 1934) or to the

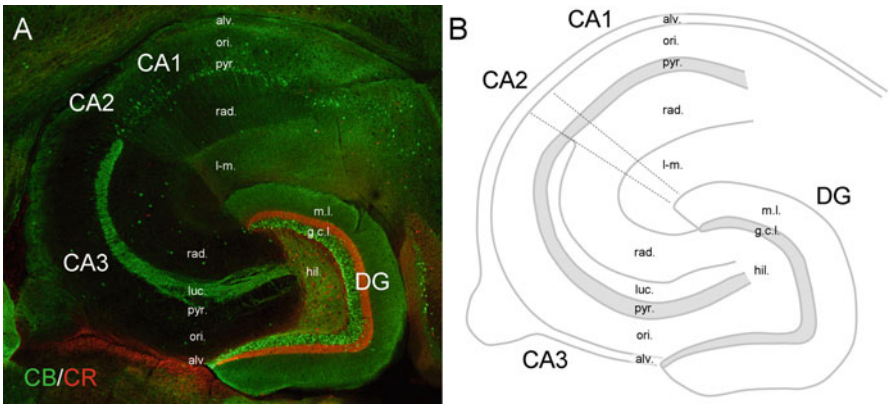

Fig. 1 Areas and layering of the hippocampus. (**a**)Transverse section from the ventral mouse hippocampus immunolabeled for the calcium-binding proteins calbindin (CB, *green*) and calretinin (CR, *red*). CB is expressed by GCs and a subset of CA1 pyramidal cells. Therefore the DG and the CA1 area show labeling of the cell bodies and a homogeneous staining of the dendritic layers. In the CA3 area, the narrow band of GC axons (the mossy fibers) is labeled in the *str. lucidum* (luc.). CR immunostaining labels mossy cells in the hilus (hil.) and delineates the termination of their axon in the inner third of the molecular layer (m.l.) of the mouse hippocampus. In addition to principal cells, a subset of interneurons scattered throughout the hippocampus can be seen labeled by either CB or CR. (**b**) Schematic drawing of the areas and layers of the hippocampus. Abbreviations: alv., alveus; ori., str. oriens; pyr., str. pyramidale; rad., str. radiatum; l-m., str. lacunosum-moleculare; g.c.l., granule cell layer. *Dashed lines* indicate borders between the CA areas

DG as a "polymorphic layer" (Blackstad 1956; Amaral 1978). Because of the tight mutual connectivity, the general consensus seems to favor the latter hypothesis, with the term CA4 no longer used. Nevertheless, the *hilus* is often silently regarded as an area on its own right.

The hippocampus displays a strict laminar structure (Förster et al. 2006; Fig. 1). Principal cells are tightly aligned and their somata form well-defined layers, the *stratum (str.) pyramidale* in the CA areas and the granule cell layer in the DG. The multiple curvatures of the hippocampus mean that the orientation of principal cells depends on their position along the septotemporal and transverse axes. Vertical positions are therefore referenced to the main axis of the principal neurons. The neuropil in the CA areas is subdivided into three major layers (from basal to apical direction): (1) the *str. oriens*, which is below the cell body layer; (2) the *str. radiatum* above the cell body layer; and (3) the *str. lacunosum-moleculare*. The *str. oriens* and *radiatum* are the innervation zones for the ipsilateral associational fibers (including the *Schaffer collaterals*) and the contralateral commissural axons originating in the CA3 areas. The *str. lacunosum-moleculare* is the layer in which the perforant and temporoammonic path axons from the entorhinal cortex terminate. The *str. lacunosum-moleculare* can be further divided into the *str. lacunosum* (being the common location of dendritic bifurcation) and the *str. moleculare* (location of distal dendritic tuft). In the CA3 area, there is an additional narrow layer, the *str. lucidum*,

immediately above the cell body layer where projections from the mossy fibers of the DG terminate (for further details on connectivity, see chapter "Connectivity of the Hippocampus"). Finally, a layer of white matter consisting of afferent and efferent axons, the alveus, is found below *str. oriens*.

In the DG, the neuropil above the granule cell layer forms the molecular layer (ML). Similar to CA3, commissural/associational axons originating primarily from hilar mossy cells terminate proximally in the inner third of the molecular layer (inner molecular layer, iML) and perforant path axons from either lateral or medial entorhinal cortex innervate the middle (mML) and the outer third (oML) of the ML, respectively. As noted above, the area beneath the cell body layer is regarded as the polymorphic layer (or hilus) of the DG; however, GCs have no basal dendrites and only their axons extend into that region.

Principal Cells

Principal cells of the hippocampus include the pyramidal cells of the CA areas, GCs of the DG, and mossy cells of the hilus, each of which is largely homogeneous, but each possesses subtle anatomical, molecular, and genetic variations.

CA1 Pyramidal Cells

Pyramidal cells of the CA1 are one of the most-investigated types of neurons in the brain. The number of pyramidal cells in the rat CA1 has been estimated to be on the order of 3.2–3.5 $\times$ 10^5 (unilateral values from male Wistar rats, Hosseini-Sharifabad and Nyengaard 2007, or Sprague-Dawley rats, Miettinen et al. 2012). These neurons are characterized by a pyramid-shaped or ovoid soma, a large-caliber apical dendrite, and a number of small-caliber basal dendrites (Fig. 2a, b). Cell bodies of CA1 pyramidal cells are typically found in the cell body layer (*str. pyramidale*) or in proximal *str. oriens*. The *str. pyramidale* of the CA1 area has been subdivided in a superficial compact layer with one to two dense rows of pyramidal cells and a deep loosely packed layer of scattered cell bodies (Lorente de Nó 1934; Slomianka et al. 2011). As mentioned above, increasing evidence indicate that CA1 pyramidal cells do not constitute a uniform cell type throughout the region, rather differ remarkably in their physiological characteristics (Graves et al. 2012). Beyond that, superficial and deep cells have been recently found to differ in their internal and external excitatory and inhibitory connectivity as well as their functional properties (Mizuseki et al. 2011; Lee et al. 2014; Masurkar et al. 2017). Moreover, a population of displaced pyramidal cells has been identified in *str. radiatum* (Cajal 1968; Gulyás et al. 1998), which possess certain unique physiological properties and projection patterns (Christie et al. 2000; Bullis et al. 2007).

The cell bodies of CA1 pyramidal cells have a diameter of $\sim$15 μm and a surface area of 465 $\pm$ 50 μm^2 (Megías et al. 2001). The apical dendrites (typically 1,

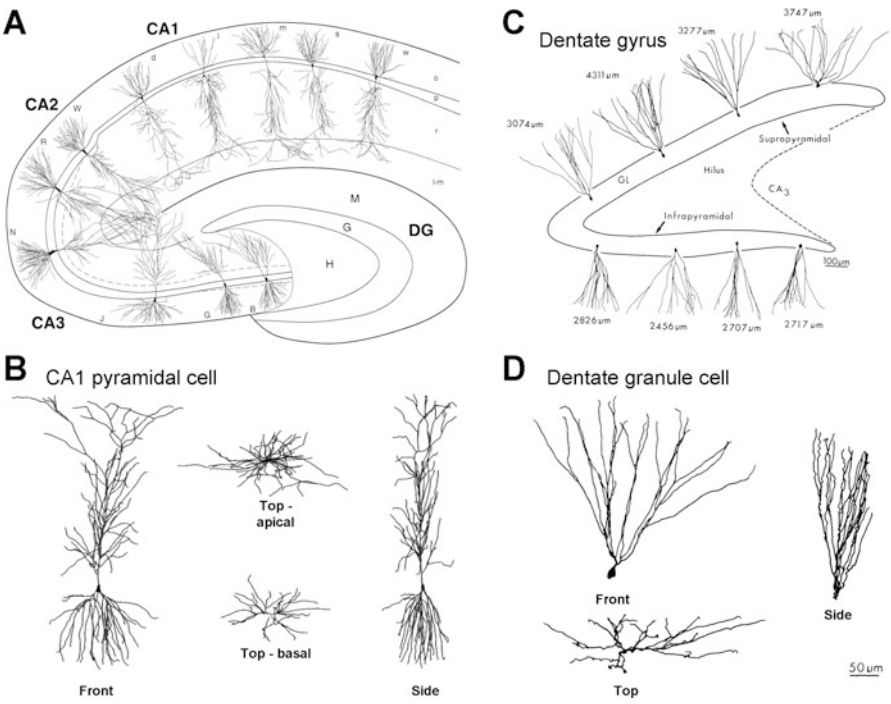

Fig. 2 Morphology of hippocampal principal cells. (**a**) Pyramidal cells of the CA1, CA2, and CA3 area. (**b**) Three-dimensional structure of a CA1 pyramidal cell illustrated from frontal, side, and top views. (**c**) Morphological diversity of DG GCs. Values adjacent to the cells indicate the total dendritic length. Note the difference between the upper (suprapyramidal) and lower (infrapyramidal) blades. (**d**) Three-dimensional structure of a GC illustrated from frontal, side, and top views (**a**, **b** from Ishizuka et al. 1995; **c**, **d** from Claiborne et al. 1990, reproduced with permission. © J. Wiley & Sons)

occasionally 2, or even 3 primary branches) extend into *str. radiatum* with between 9 and 30 oblique side branches in this layer (Bannister and Larkman 1995a). They end with a bifurcation at the border of *str. radiatum* and *str. lacunosum* and form a dendritic tuft in *str. lacunosum-moleculare*. Two to eight basal dendrites emerge from the base of the cell body in the *str. oriens*. These dendrites bifurcate repeatedly close to the soma and the long terminal branches run toward the alveus.

The total dendritic length of CA1 pyramidal cells has been reported to be in the range of 11.5 and 17.5 mm (Table 1). The considerable variability could be due to differences in the strain, sex, and age of the rats, as well as the experimental approach used in the studies (i.e., in vitro vs. in vivo labeling, correction for shrinkage). Corresponding estimates of the somatodendritic surface area are 28,860 and 36,000 μm^2, excluding dendritic spines (Bannister and Larkman 1995b, Cannon et al. 1999; Table 1). However, dendrites of CA1 pyramidal cells are densely covered with spines and they can significantly influence the calculated surface area.

Table 1 Dendritic length and somatodendritic surface area of CA1 pyramidal cells

Layer	Dendritic length (μm)	% of dendrites	Surface area (μm^2)	Reference/rat strain, age
Total	13,424 ± 1061			Ishizuka et al. (1995)
L-M	2531 ± 571	18.8%		Sprague-Dawley, 33–57 days
Rad	6307 ± 975	47.0%		In vitro labeling
Ori	4586 ± 935	34.2%		
Total	16,300 ± 4330			Pyapali et al. (1998)
Apical	11,300 ± 4080	69.5%		Fischer 344, 2 months
Basal	5070 ± 1160	30.5%		In vitro labeling
Total	17,400 ± 3900			Pyapali et al. (1998)
Apical	10,600 ± 2450	60.9%		Sprague-Dawley, 2–8 months
Basal	6890 ± 2110	39.1%		In vivo labeling
Total	11,915 ± 1030		28,860 ±3102	Bannister and Larkman (1995a)
L-M	2259 ± 526	19%		Sprague-Dawley, male 100–150 g
Rad	4118 ± 1203	35%		In vitro labeling
Ori/Pyr	5538 ± 943	47%		
Total	17,400 ± 6200		36,100 ± 17,00	Cannon et al. (1999)

				Sprague-Dawley, 2–8 months In vivo labeling
Total	11,549 ± 2010			Megías et al. (2001)
L-M	2712 ± 873	23.5%		Wistar, male, ~300 g
Rad	4638 ± 1022	40.2%		In vivo labeling
Ori/Pyr	4198 ± 1056	36.3%		
Total	12,808 ± 1541		67,102 ± 10,953	Ambros-Ingerson and Holmes (2005) adapted from Carnevale et al. (1997)
Apical	7943 ± 1526	62%		Sprague-Dawley, 42–368 days
Soma	40 ± 9	0%		In vitro labeling
Basal	4826 ± 995	38%		
Total	14,472 ± 2539			Buckmaster (2012) Sprague-Dawley, adults In vivo labeling
Total	8810 ± 1719		64,208 ± 15,087	Degro et al. (2015) Wistar, 3–4 weeks In vitro labeling

Values are mean ± S.D. Surface area is given without spines

The total number of spines has been estimated to be over 30,000 (Bannister and Larkman 1995b, Megías et al. 2001; see Table 2). Bannister and Larkman (1995b) calculated that spines increase the dendritic surface area by a factor of 0.89 in CA1 pyramidal cells. The distribution of spines is not homogeneous on the dendritic surface: spine density is highest in *str. oriens* and *radiatum* with values between 1.26 and 1.43 μm^{-2} and lower with 0.6 μm^{-2} in *str. lacunosum-moleculare* (Bannister and Larkman 1995b). These surface density values correspond to a linear, length density of 7.5 μm^{-1} on the apical trunk, 2.4–3.2 μm^{-1} on basal and oblique dendrites, and 1.4 μm^{-1} on dendrites of the apical tuft (Bannister and Larkman 1995b); these values are in good agreement with electron microscopic estimates of spine density (Harris et al. 1992). Interestingly, spines in *str. lacunosum-moleculare* are more often contacted by the same presynaptic axon, forming clustered synapses, than for *str. radiatum* spines (Bloss et al. 2018).

Spines serve as postsynaptic targets primarily for glutamatergic terminals; therefore their high numbers indicate a massive excitatory synaptic input to these cells. In fact, in a detailed morphological study, Megías et al. (2001) showed that on average ~30,600 terminals converge and form asymmetrical, putative excitatory synapses onto a single CA1 pyramidal cell in the rat (Table 2), whereas in the mouse, this value is substantially lower on the order of 10,000 (Bloss et al. 2016; Table 3). Over 99% of these asymmetrical synapses are located on dendritic spines, although in the *str. lacunosum-moleculare*, up to 17% of the synapses can be found on dendritic shafts. Somata of pyramidal cells are devoid of excitatory synapses (Fig. 3). Interestingly, superficial and deep pyramidal cells in the mouse differ with respect to the density of spines in s*tr. lacunosum-moleculare:* deep pyramidal cells have 50% fewer spines in CA1a corresponding to fewer medial entorhinal cortex inputs, whereas in CA1c deep pyramidal cells have higher spine density, reflecting a higher incidence of medial entorhinal inputs (Masurkar et al. 2017).

The number of symmetrical, putative inhibitory synapses formed by GABA-immunopositive boutons is much lower. A single neuron receives ~1700 symmetrical synapses, which correspond to only 5.6% of the total number (Megías et al. 2001). In contrast to excitatory synapses, a large proportion (40%) of inhibitory synapses are found in the perisomatic domain, with 7% of the synapses located on the soma and the axon initial segment and 33% on proximal dendrites. In these compartments, inhibitory synapses comprise 50–100% of all synapses. In contrast, on dendrites in the *str. radiatum* and *oriens*, the proportion of these synapses is only 4–5%. Interestingly, on distal apical dendrites in the *str. lacunosum-moleculare*, the proportion increases again to 16% (see Table 2). On the dendrites, almost all (>98%) inhibitory terminals form contacts with shafts. However, as an exception to this rule, in the str. lacunosum-moleculare, 10–20% of the inhibitory synapses have been found on spines (Megías et al. 2001).

The axon of CA1 pyramidal cells with origin at the axon initial segment (AIS) emerges from either the soma or a proximal dendrite, with equal likelihood (Thome et al. 2014). Action potentials are preferentially generated in AIS, with the initiation site localized in the distal half, and backpropagate to the soma and dendrites (Stuart and Sakmann 1994; Palmer and Stuart 2006). If the AIS is found on a dendrite,

Table 2 Laminar distribution of excitatory and inhibitory synapses on CA1 pyramidal cells in the rat

Layer	Spines	% of total	Synapses	GABA(−) synapses	% within layer	GABA(+) synapses	% within layer
Total	30,382 ± 5214		32,351 ± 5486	30,637 ± 5259	94.7%	1713 ± 261	5.3%
L-M	1521 ± 541	5.0%	2110 ± 726	1776 ± 613	84.2%	334 ± 113	15.8%
Rad	16,878 ± 3964	55.6%	17,619 ± 4085	16,878 ± 3964	95.8%	741 ± 126	4.2%
Ori	11,982 ± 3164	39.4%	12,621 ± 3292	11,982 ± 3164	94.9%	639 ± 147	5.1%
Soma	N/A	N/A	92 ± 12	0	0%	92 ± 12	100%
AIS	N/A	N/A	24 ± 2	0	0%	24 ± 2	100%

Percentage values for the spines indicate the proportions found in the different layers; percentages after synapse numbers indicate the proportion of putative excitatory GABA-immunonegative (GABA(−)) and GABA-positive (GABA(+)) synapses. Data from Megías et al. (2001)

Table 3 Laminar distribution of excitatory and inhibitory synapses on CA1 pyramidal cells in the mouse

Layer	Spines	% of total	GABA(+) synapses	% within layer
Total	9537		560	5.3%
L-M	1300	13.6%	287 (51,3%)	51.3%
Rad	4998	52.4%	113 (20,2%)	20.2%
Ori	3239	34.0%	160 (28,6%)	28.6%
Soma	N/A			
AIS	N/A			

Values represent estimated numbers of synapses D. Percentage values for the spines indicate the proportions found in the different layers. Data from Bloss et al. (2016)

action potentials will occur earlier in the "privileged" dendrite than in the soma or other dendrites of the neuron (Thome et al. 2014). The main axon collateral runs in the alveus and is directed toward the fimbria/fornix, forming long-range connections with the subiculum, entorhinal cortex, amygdala, prefrontal cortex, as well as many other cortical regions (see chapter "Connectivity of the Hippocampus"). Although the extent of local arborization is limited, axon collaterals are present in the *str. oriens* and to a lesser degree in the radiatum. These collaterals provide a major excitatory input to interneurons providing feedback inhibition, in particular to somatostatin-immunopositive O-LM interneurons (Blasco-Ibáñez and Freund 1995; Katona et al. 1999a; Csicsvari et al. 1998; Maccaferri et al. 2000) but other interneuron subtypes as well (Ali and Thomson 1998, Takács et al. 2012). Additionally, these collaterals also form synapses onto neighboring pyramidal cells; however this recurrent connectivity in the CA1 area is very low at only ∼1% (Deuchars and Thomson 1996).

Positional Differences in the Anatomical, Molecular, and Functional Properties of CA1 Pyramidal Cells Along the Medio-Distal and Septotemporal Axes

CA1 pyramidal cells were long considered to constitute a largely homogeneous population; however, increasing evidence points to a stronger heterogeneity of these neurons. In particular, position-dependent effects were observed along all three

Fig. 3 (continued) In the *str. lacunosum-moleculare*, three subclasses of dendrites were identified on the basis of diameter and spine density: thick dendrites possessed fewer spines (l-m/thick), intermediate sparsely spinous (l-m/medium), and more distal thin and nearly spine-free dendrites (l-m/thin). For every dendritic subclass, the density of asymmetrical, putative excitatory and symmetrical, putative inhibitory synapses (*boxes*, left and middle numbers, respectively [μm^{-1}]) and the proportion of symmetrical synapses (*boxes*, right number) are shown. Values below the *boxes* indicate total length (mean ± S.D.) and diameter (mean and range in μm) (Modified from Megías et al. 2001 with permission. © Elsevier)

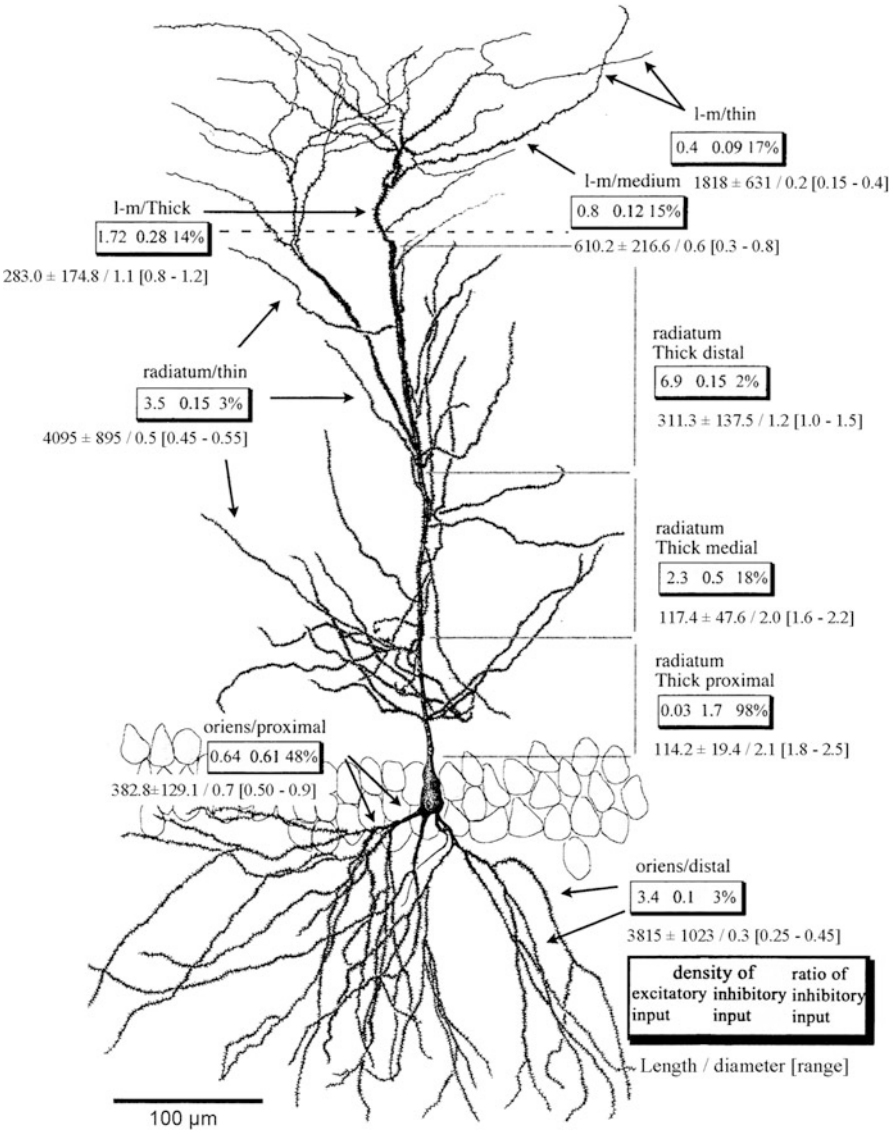

Fig. 3 Distribution of synapses on the dendrites of CA1 pyramidal cells. The drawing illustrates the subclasses of dendrites distinguished in the study by Megías et al. (2001). In the *str. oriens*, two types of dendritic processes were classified: first-order proximal basal dendrites with low spine density (oriens/proximal) and higher-order distal dendrites with high spine density (oriens/distal). In the *str. radiatum*, four subclasses of dendrites were distinguished. The thick apical dendritic trunk was divided into three segments: a proximal part with no spines (radiatum/thick/proximal), a medial sparsely spiny part (radiatum/thick/medial), and a densely spiny distal part (radiatum/thick/distal). The fourth type corresponds to the thin oblique side branches (radiatum/thin).

axes of the CA1 area in terms of anatomical, molecular, and functional properties of pyramidal cells. In fact, Lorente de Nó in his early study of the hippocampus introduced the "a, b, and c" subdivisions of the CA1 area along the transverse axis based on differences in the anatomical connectivity of pyramidal cells (Lorente de Nó 1934; see chapter "Connectivity of the Hippocampus"). More recent in vitro and in vivo electrophysiological studies revealed further divergence in the intrinsic properties, discharge pattern, and place field properties along this axis (Igarashi et al. 2014). Furthermore, as noted above, superficial and deep cells differ in their internal and external excitatory and inhibitory connectivity (Mizuseki et al. 2011; Lee et al. 2014; Masurkar et al. 2017).

Similar but not tightly correlated gradients were observed in neurochemical properties of CA1 pyramidal cells, in particular in the expression of the calcium-binding protein calbindin (CB, see Fig. 1), which labels a subset of CA1 PCs. In proximal CA1 (i.e., the CA1c, closest to CA2), a relatively sparse population of pyramidal cells is labeled, while in distal CA1 (CA1a, closest to subiculum), almost all neurons express CB (Sloviter 1989). The functional ramifications of the CB are yet to be fully understood, but the absence of CB leads to reduced plasticity and impaired synaptic transmission (Jouvenceau et al. 1999). Interestingly, only very few CA2 pyramidal cells are labeled for CB and almost no CA3 neurons either. However, CB strongly labels mature dentate GCs and their axons, suggesting strong calcium sequestration in mossy fiber axons (Dumas et al. 2004).

Genetic analysis, in particular single-cell reverse-transcriptase PCR and RNA sequencing, at the level of the population and single cells, has further revealed a diversity of principal cell populations, with respect to hippocampal position and cell type (Cembrowski et al. 2016a, b; Fig. 4). This approach is redefining our understanding of molecular composition in ways not possible in earlier studies, producing exhaustive lists of neurochemical diversity within and between principal cell types. One notable example is the divergence of CA1 pyramidal cells along the dorsoventral axis of the hippocampus in terms of RNA expression gradients (Fig. 4b), which is also reflected in their physiological and morphological properties (Dougherty et al. 2012, 2013; Cembrowski et al. 2016a; Milior et al. 2016; Ruchi et al. 2016; Fig. 5).

The list of known genes differing between different principal cell types is ever increasing, with the known unique genes and proteins (see Table 4). Despite many of these genes being associated with synaptic and intrinsic physiology, numerous of the alternatively expressed genes are associated with cytoskeletal elements and growth/transcription factors. For example, this genetic anatomical approach, thus, reveals a greater subdivision of hippocampal subregions and helps to define their borders (Thompson et al. 2008), plausibly reflecting functional differences. While the role that these alternative gene expression patterns play in divergent morphology and connectivity of principal cells is yet to be fully understood, they could serve as markers as well as targets for genetic manipulations in future attempts to understand

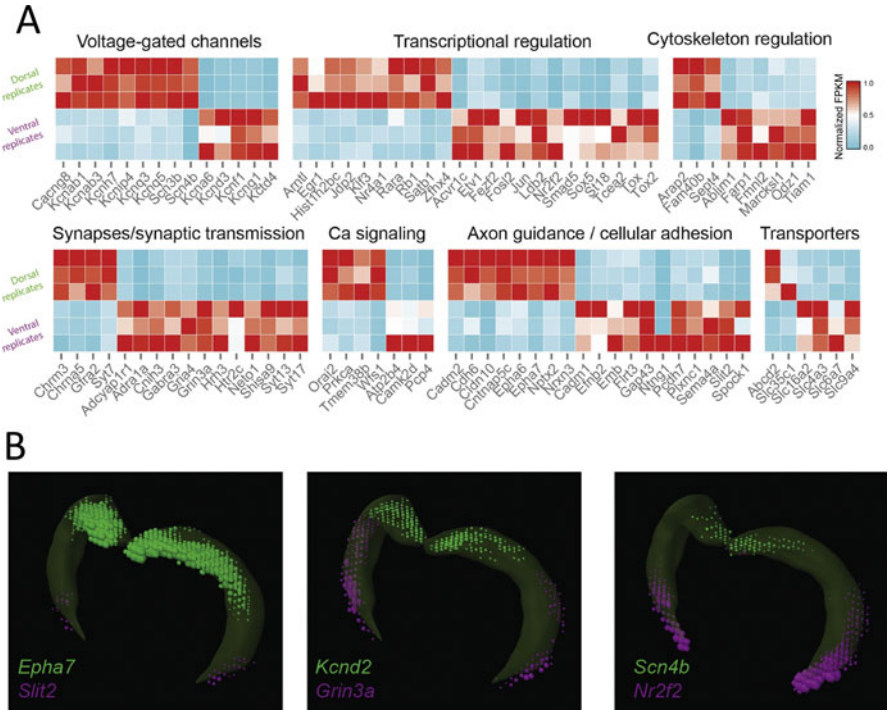

Fig. 4 Differential gene expression patterns along the dorsoventral axis of the CA1 area of the hippocampus. (**a**)**,** A subset of genes enriched in a pole-specific fashion with neuronal relevance. Top and bottom three rows depict dorsal and ventral replicates, respectively. Range is normalized to the highest replicate FPKM on a gene-by-gene basis. (**b**)**,** Regionally restricted gene expression along the dorsoventral axis of the CA1 area from the Allen *Brain* Atlas Brain Explorer. CA1 areas of the left and right hippocampi are shown in green. Genes identified were involved in neurotransmission (Grin3a), transcriptional regulation (Nr2f2), intrinsic excitability (Kcnd2, Scn4b), and axon guidance (Epha7, Slit2). (Adapted from Cembrowski et al. 2016a with permission. © Cell Press)

functional relevance of the identified neurons and the molecules (Cembrowski et al. 2016b; Mikulovic et al. 2015).

CA3 Pyramidal Cells

The number of pyramidal cells of the CA3 area is substantially lower at $1.88 \pm 0.02 \times 10^5$ than that of CA1 neurons (male Wistar rats, Hosseini-Sharifabad and Nyengaard 2007). In their morphology, CA3 pyramidal cells show many similarities to CA1 pyramidal cells; however, there are a number of notable differences. The cell bodies are larger and have a surface area approximately 2–4 times higher than that of CA1 pyramidal cells. The apical dendrites bifurcate closer to *str. pyramidale* and often two or three apical dendrites emerge from the apical pole of the elongated

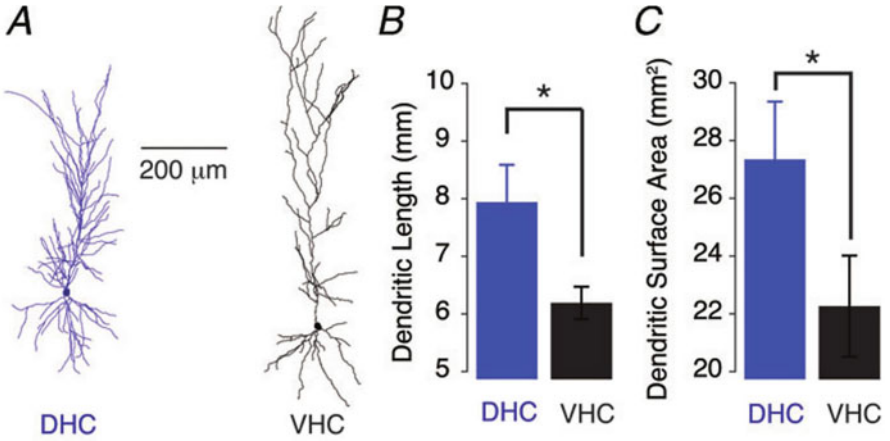

Fig. 5 Morphological differences between CA1 PCs from the dorsal (DHC) and ventral hippocampal (VHC). (**a**)**,** Representative morphological reconstructions of a DHC (left) and a VHC (right) pyramidal neuron. (**b, c**)**,** Summary bar charts of the total dendritic length (**b**) and surface area (**c**) indicate significantly greater dendritic arbor for DHC neurons than VHC neurons (Wilcoxon RS tests, $P < 0.05$). (Reproduced from Dougherty et al. 2012 with permission. © Wiley-Blackwell)

soma. Finally, proximal dendrites of CA3 pyramidal cells bear large complex spines ("thorny excrescences"); these complex spines are the postsynaptic targets of mossy fiber boutons (Blackstad and Kjaerheim 1961; Frotscher et al. 1994; Claiborne et al. 1986; Chicurel and Harris 1992; Acsády et al. 1998).

The total dendritic length of CA3 pyramidal cells (Table 5) is comparable to that in the CA1 area. However, the cell-to-cell variability is higher, partially due to structural differences along the transverse axis of the CA3 (Ishizuka et al. 1995; Turner et al. 1995); estimates of the somatodendritic surface without spines range between 22,033 and 50,400 μm2 (Henze et al. 1996; Cannon et al. 1999). Spines enlarge the dendritic surface by a factor of 0.88 (based on data by Major et al. 1994, Table 5). The density (2.9 $\mu m-1$) and total number (33,200) of spines are also similar to those in the CA1 area (Major et al. 1993).

Complex spines are found in small clusters on the proximal apical dendrite in the *str. lucidum*, corresponding to the termination zone of mossy fibers (Gonzales et al. 2001). In the CA3c, where mossy fibers form an infrapyramidal bundle, spines can also be found on the proximal basal dendrites. Due to limitations of light microscopy, the resolution of individual spines is difficult, but estimates suggest that the number of complex spines on a single CA3 pyramidal cell can be up to 41 (Gonzales et al. 2001). As each complex spine is contacted by a single mossy fiber bouton (Chicurel and Harris 1992; Acsády et al. 1998), this number defines the convergence of GCs onto CA3 pyramidal cells. Although there is only limited information about other excitatory synaptic inputs to CA3 pyramidal cells, the distribution of dendrites and the number of spines suggest that the total

Table 4 A non-exhaustive list of known cell-type specific genes in hippocampal principal cells, organized by broad function

Region	Cytoskeletal	Signaling	References
CA1	*Col5a1*[3] (collagen formation)	*Wfs1*[1,3] (Ca^2+ signaling)	[1]Luuk et al. (2008)
	Dcn[3] (collagen formation)	Calbindin [2] (Ca^{2+} signaling)	[2] Sloviter (1989)
	Matn2[3] (ext. cellular matrix)	*Grp*[3] (neuropeptide)	[3]Dong et al. (2009)
	Fbln2[3] (ext. cellular matrix)	*Lct*[3] (lactase)	
CA2	Alpha actinin 2 (actin cross-linking)	*PCP4* (calmodulin binding)	Botcher et al. (2014)
CA3	*Itga7* (cell adhesion)	*Fmo1* (metabolism)	Thompson et al. (2008)
	Coch (neurite outgrowth)	*Mas1* (7-TM)	
	Loxl1 (ext. cellular matrix)	*Plagl1* (DNA binding)	
		Ptgs2 (mitochondrial)	
Mossy cell	p11 (scaffold and transport)	mGluR2/3 (7-TM)	Scharfman (2016)
	Dysbindin 1C (axon growth)	Calretinin (Ca^{2+} signaling)	
		CGRP (neuropeptide)	
		STEP (tyrosine phosphatase)	
GC	Dysbindin (axon)	Calbindin (Ca^{2+} signaling)	
	Prox1 (maturation)	Glucocorticoid R2 (receptor)	
	Tuj1 (cytoskeleton)	mGluR2/3 (7-TM)	
Adult-born GC	Doublecortin (differentiation)		Seri et al. (2004)
	Reelin (differentiation)		
	NeuroD (differentiation)		

Table 5 Dendritic length and somatodendritic surface area of CA3 and CA2 pyramidal cells

Layer	Dendritic length (μm)	% of dendrites	Surface area (μm^2)	Reference/rat strain, age
CA3c ($n = 4$)				Major et al. (1994)
Total	11,169 ± 878a		59,900 ± 4738	Wistar, 18–21 days
Dendrites			30,600 ± 4700	In vitro labeling
Dendrites with spines			57,600[a]	
Soma			2300 ± 600	
Axon			22,600 ± 3000	
CA3 ($n = 20$)				Ishizuka et al. (1995)
Total	12,482 ± 2999			Sprague-Dawley, 33–57 days
L-M	1983 ± 458	15.9%		In vitro labeling
Rad	4382 ± 975	35.1%		
Luc/Pyr	471 ± 250	3.8%		
Ori	5646 ± 1745	45.2%		
CA3a ($n = 4$)				Turner et al. (1995)
Total	19,800 ± 2030			Sprague-Dawley, 2–8 months
CA3b ($n = 4$)				In vitro labeling
Total	19,100 ± 2330			
CA3c ($n = 4$)				
Total	10,400 ± 720			

CA3b ($n = 8$)				Henze et al. (1996)
Total	11394 ± 1735		22,033 ± 3559	Sprague-Dawley, 28–35 days
Apical	6332 ± 1029	55.6%	12,629 ± 3556	In vitro labeling
Basal	5062 ± 1397	44.4%	9404 ± 4958	
CA3 ($n = 15$)				Cannon et al. (1999)
Total	18,100 ± 8600		50,400 ± 24,000	Sprague-Dawley, 2–8 month, in vivo labeling
CA3 (n=9)				Buckmaster (2012), Sprague-Dawley, adult
Total	8804 ± 2224			In vivo labeling
CA3 (n=5)				Degro et al. (2015)
Total	7730 ± 1791		41,422± 8840	Wistar, 3–4 weeks
				In vitro labeling
CA2 ($n = 14$				Ishizuka et al. (1995)
Total	15,406 ± 950			Sprague-Dawley, 33–57 days
L-M	4672 ± 293	30.3%		In vitro labeling
Rad	4799 ± 732	31.1%		
Pyr	71 ± 34	0.5%		
Ori	5865 ± 491	38.1%		

number of synapses made by commissural/associational and perforant path axons is comparable to the numbers obtained for the pyramidal cells of the CA1 area.

The axon of CA3 pyramidal cells typically emanates from the soma or a proximal dendrite, with 30% of AIS's being found on a dendrite (Thome et al. 2014). Of note, the AIS of CA3 PCs possesses axonal protrusions (similar to dendritic spines), which were contacted by between 1 and 5 inhibitory synapses and occasionally also excitatory synapses (Kosaka 1980). The main axonal projection is to the ipsi- and contralateral hippocampi, forming the commissural/associational pathways to the CA3, CA2, and CA1 areas; the latter is referred to as the "Schaffer collaterals" (Ishizuka et al. 1990; Li et al. 1994). However, there are also collaterals, mostly arising from the CA3c, which are directed to the hilus and the DG (Li et al. 1994; Scharfman 2007). The length of the axon ipsilaterally ranges between 150 and 300 mm and may contact up to 30,000–60,000 postsynaptic neurons (Li et al. 1994). A recent in vivo labeling study found that the total axonal length of a single CA3 pyramidal cell was more than 0.5 m, covering almost two-thirds of the septotemporal extent of the area (Wittner et al. 2007). The majority of target cells (85%) are innervated through a single synaptic contact (Sík et al. 1993; Gulyás et al. 1993b). Axons originating in the CA3a area terminate to a larger degree in the CA3 than in the CA1 area (ratio 3:1), whereas for the CA3c area, the termination pattern is inverse (ratio 1:3, Li et al. 1994). Thus, local targets of a single CA3 pyramidal cell may vary between ~7500 and 45,000 (i.e., 5–30% of the ~150,000 neurons comprising the CA3 population). Postsynaptic targets include feedforward interneurons, such as parvalbumin-containing basket cells, in proportion to their occurrence (Sík et al. 1993; Gulyás et al. 1993b; Wittner et al. 2006).

Similar to the results obtained for the CA1, morphological and genetic analysis of CA3 pyramidal cells reveals divergence along both the medio-distal and the dorsoventral axis of the hippocampus (Ishizuka et al. 1995; Turner et al. 1995; Thompson et al. 2008).

CA2 Pyramidal Cells

CA2 area was defined by Lorente de Nó (1934) as a small, distinct region between the CA1 and CA3 based on its cytoarchitectural features. More recent analyses of gene expression further demonstrated that CA2 area can be reliably identified by selective molecular markers, including Purkinje cell protein 4 (PCP4), regulator of G protein signaling 14 (RGS14), STEP, and MAP3K15, indicating a wider region (~300 μm) than what was cytoarchitecturally defined (~100 μm) (Lein et al. 2005; Lee et al. 2010; Kohara et al. 2014).

CA2 pyramidal cells show morphological features in between those of the CA1 and CA3 areas. Cell bodies of these neurons have similar size as those of CA3 pyramidal cells, and 2–3 times larger than CA1 pyramids, but the cells lack complex spines and their dendritic arborization pattern is more similar to that of CA1 pyramids (Ishizuka et al. 1995; Mercer et al. 2007). Quantitative analysis of the dendrites of in vitro labeled neurons indicates that CA2 pyramidal cells have the

highest total dendritic length compared to CA1 and CA3 pyramidal cells in the same study (Ishizuka et al. 1995; but see Mercer et al. 2007). The difference is primarily due to the higher length of dendrites in the *str. lacunosum-moleculare*, whereas in the *str. radiatum* and *oriens*, values are comparable (Ishizuka et al. 1995; Table 5). In fact, the dendritic arborization pattern of CA2 pyramidal neurons differ from those of CA1 cells, in that the primary apical dendrite divides into several secondary branches relatively close to the soma. The secondary branches give rise to very few oblique branches in *str. radiatum* but extend deep into the *str. lacunosum-moleculare* (Srinivas et al. 2017).

There is little information on the synaptic connectivity of these neurons. Two major excitatory inputs are the commissural/associational fibers and the perforant path with similar termination as in the CA1 and CA3 areas. However, they have over twofold higher spine density, which, combined with a higher total dendritic length, results in a near threefold larger entorhinal input (Srinivas et al. 2017). However, the entorhinal input appears to originate from layer II but not from layer III neurons (Kohara et al. 2014). In addition, the CA2 region receives a strong input from the supramammillary nucleus (Maglóczky et al. 1994; Kohara et al. 2014). Finally, despite their lack of complex spines, CA2 pyramidal cells have excitatory synaptic input from the DG via the mossy fibers (Kohara et al. 2014). Inhibitory innervation of the CA2 area is similar to both CA1 and the CA3 (Mercer et al. 2007); however CA2 contains many more PV and Reelin immunopositive interneurons than either CA1 or CA3 (Botcher et al. 2014). Axons of CA2 pyramidal cells, similar to CA3 pyramids, project to the ipsi- and contralateral CA1–3 areas contributing to the commissural/associational system (Tamamaki et al. 1988; Li et al. 1994; Mercer et al. 2007). The ipsilateral length of axons was measured to be ~150 mm, further indicating that not only the distribution but also the number of postsynaptic targets is comparable to those of CA3 pyramids (Li et al. 1994). In contrast to CA3 pyramidal cells, however, CA2 neurons preferentially project to deep CA1 pyramidal cells (Kohara et al. 2014).

DG Granule Cells

DG possesses a large population of unique principal cell type, the GCs, which markedly differ in their anatomical properties from pyramidal cells of the CA areas. The number of GCs has been estimated to be on the order of 10^6 ($1.08 \pm 0.09 \times 10^6$, unilateral value, male Wistar rats, Hosseini-Sharifabad and Nyengaard 2007). GCs show a moderate diversity, due in part to the fact that GCs are one of only two known populations of adult-born neurons (Cameron et al. 1993, 2001); as a result the population of mature GCs is interspersed with immature GCs with divergent morphologies (Zhao 2006). GCs are characterized by a strictly bipolar morphology: spiny dendrites originate from the upper pole of the soma and an axon emerges from the base (Fig. 2c, d; Seress and Pokorny 1981; Claiborne et al. 1990; Schmidt-Hieber et al. 2007). Mature GCs have small, round, or ovoid cell bodies with a diameter of ~10 μm and are located densely packed in the GC layer most

proximal to the ML. One to four primary dendrites arise from the soma, bifurcating 3–6 times to form a dendritic tuft in the ML. Terminal branches extend mostly to the hippocampal fissure, and the tuft occupies a conical-shaped volume within the ML with a wider transverse (~300 μm) and a narrower (~180 μm) septotemporal extent. Dendrites show a gradual taper with diameters changing from ~1.5 μm on proximal dendrites to 0.7 μm on distal dendrites (Schmidt-Hieber et al. 2007). The total dendritic length ranges between 2324 and 4582 μm, thus, substantially shorter than for pyramidal cells (Claiborne et al. 1990; Table 6). Quantitative differences exist between GCs of the upper and the lower blades, as well as between superficial (near the molecular layer) and deep cells (near the hilus; Claiborne et al. 1990). However other studies have failed to confirm these differences (Beining et al. 2017). Superficial neurons in the upper blade have the highest total dendritic length and the widest arbor, whereas deep neurons in the lower blade have the shortest length and the narrowest transverse extent (Table 6).

Similar to pyramidal cells, mature GC dendrites are densely covered with spines. The total number was calculated to be between 3091 and 6830 on the basis of a light microscopic estimate of spine density ($2.39 \pm 0.06\ \mu m^{-1}$; Schmidt-Hieber et al. 2007). Electron microscopic investigation obtained similar density values and indicated moderate differences between proximal ($3.36 \pm 0.35\ \mu m^{-1}$), mid-distal ($2.88 \pm 0.33\ \mu m^{-1}$), and distal ($2.02 \pm 0.28\ \mu m^{-1}$) dendritic segments (Hama et al. 1989). The differences in the density are largely explained by the decreasing diameter and surface area of proximal to distal dendrites. In fact, the surface density of spines was comparable in the dendritic compartments with values ranging from 0.79 to 0.88 μm^{-2} (Hama et al. 1989). Spine surface contributes by a factor of 0.91–1.05 to the total surface area of the neurons (Schmidt-Hieber et al. 2007; Hama et al. 1989).

There are only limited quantitative data on the synaptic inputs to GCs. The number of excitatory synapses can be estimated on the basis of spine densities. The three main afferent systems, the commissural/associational path, the medial and the lateral perforant path, terminate in a strictly laminated fashion in the inner, middle, and outer molecular layers, respectively. The proportions of the dendrites falling into these layers are ~30, 30, and 40% (Claiborne et al. 1990; Schmidt-Hieber et al. 2007). The corresponding spine numbers on the surface of GCs with a dendritic length of ~3200 μm (Claiborne et al. 1990), calculated using the spine density estimates of Hama et al. (1989; see above), are 3250, 2780, and 2600. Thus, the number of excitatory synapses onto a single GC could be as high as 8630.

The distribution of inhibitory terminals was analyzed in a combined immunocytochemical and electron microscopic study (Halasy and Somogyi 1993a). Results indicate that in the molecular layer, ~7.5% of the synapses are GABA-immunopositive, and these synapses comprise 75% of all inhibitory synapses, with the remaining 25% located in the cell body layer. Therefore, the number of inhibitory synapses onto a single granule cell can be estimated as ~860, with ~650 in the molecular layer and ~190 in the cell body layer. The compartmental distribution of the inhibitory input is broken down to 63–73% dendritic shafts and 27–37% spines in the molecular layer. In the cell body layer, the majority, between

Table 6 Dendritic length and spine numbers of dentate GCs

Dendritic segments	Dendritic length (μm)	Surface (μm^2)[a]	Spine number (density [μm^{-1}])	Region	Reference Rat/Mouse strain, age
29 ± 1	3221 ± 78			Pooled data	Claiborne et al. (1990)
31 ± 1	3484 ± 130			Upper superficial	Sprague-Dawley rat, 35–49 days
30 ± 1	3468 ± 92			Upper, deep	In vitro labeling
28 ± 1	2875 ± 95			Lower, superf.	
25 ± 1	2629 ± 86			Lower, deep	
32 ± 3	2264 ± 133	13,300 ± 900			Schmidt-Hieber et al. (2007) Wistar rat, 2–4 months, in vitro labeling
24 ± 5	1985 ± 160		2254 ± 317 (1.14 ± 0.15)	Pooled	Vuksic et al. (2008)
	362 ± 53		487 ± 121 (1.34 ± 0.12)	iML	Mouse, Thy1-GFP C57BL/6 background male, 3–4 months
	1482 ± 114		1701 ± 145 (1.14 ± 0.11)	oML	

(continued)

Table 6 (continued)

Dendritic segments	Dendritic length (μm)	Surface (μm^2)[a]	Spine number (density [μm^{-1}])	Region	Reference Rat/Mouse strain, age
21 ± 2	1912 ± 90		2272 ± 252 (1.19 ± 0.12)	Dorsal DG	
	357 ± 36		486 ± 104 (1.36 ± 0.18)	iML	
	1475 ± 102		1741 ± 156 (1.18 ± 0.12)	oML	
29 ± 1	2106 ± 197		2233 ± 473 (1.06 ± 0.18)	Ventral DG	
	369 ± 80		488 ± 143 (1.32 ± 0.16)	iML	
	1486 ± 118		1664 ± 143 (1.12 ± 0.11)	oML	
	3337 ± 149			Pooled data	Buckmaster (2012), Sprague-Dawley rats, adults
					In vivo labeling
	3662 ± 88			Pooled data	Desmond and Levy (1982)
	4000 ± 215,7	9010 ± 642,4		Pooled data	Cannon et al. (1999), Sprague-Dawley rats (2–8 months), in vivo labeling
	3152 ± 323	16,271 ± 1501		Pooled data	Degro et al. (2015), Wistar, 3–4 weeks
					In vitro labeling

Values are mean ± S.E.M. Abbreviations: upper/lower, GCs in upper/lower bade; superf./deep, superficial/deep part of the granule cell layer; IML/OML, dendrites in the inner/outer molecular layer

[a]Surface area includes the axon and spines

46 and 60%, are on somata, 25–28% on proximal dendritic shafts, 7–14% on spines, and 7–9% on axon initial segments (Halasy and Somogyi 1993a).

The axons of GCs, the so-called mossy fibers, provide the major output of the DG to the CA3. The unique features of mossy fibers are the 10–18 sparsely spaced large varicosities (4–10 μm) or mossy fiber boutons that form synaptic contacts with complex spines of CA3 pyramidal cells in the *str. lucidum* and mossy cells in the hilus (Claiborne et al. 1986; Frotscher et al. 1994; Acsády et al. 1998; Rollenhagen et al. 2007). Furthermore, mossy fibers innervate a large number of inhibitory interneurons (Blasco-Ibáñez et al. 2000) in both regions through small, en passant boutons (0.5–2 μm) and filopodial extensions emerging from the large boutons, outnumbering of CA3 PCs contacted by 10:1 (Acsády et al. 1998), suggesting that the mossy fiber may predominantly drive net inhibition.

A further subtype of GC was recently described, the so-called semilunar granule cell (SLGC), which is predominantly found within the proximal iML. Despite similar dendritic branching to regular GCs, SLGCs have a greater lateral extent of their dendritic tree (420.3 ± 26.8 for SLGCs compared to 284.9 ± 33.7 μm for GCs). Their often ovoid somata give rise to their name. SLGCs surprisingly have axon collaterals which innervate the iML, forming an average of 1.8 branches in this region, suggesting a role in feedback excitation onto other GCs. SLGCs possess unique intrinsic excitability, as compared to typical GCs, and receive a strong excitatory input from hilar mossy cells (Williams et al. 2007).

Adult-Born GCs

Immature, or adult-born, GCs are found on the border of the hilus and GCL. During the weeks following neurogenesis, their dendrites are growing through the ML (Kempermann et al. 2004), with dendritic lengths of ~300 μm at 2 weeks reaching full penetration of the ML by 3 weeks (Zhao 2006). Spines do not develop on these adult-born GCs until 16 days post-differentiation, and they show strongly reduced glutamatergic inputs from all entorhinal inputs (Dieni et al. 2016), but with a strong input from hilar mossy cells (Vivar et al. 2012). The axon of adult-born GCs has already infiltrated CA3 by 10 days post-differentiation (Zhao 2006) and can drive strong inhibition (Drew et al. 2016).

Hilar Mossy Cells

Mossy cells share some morphological features with CA3 pyramidal cells. In particular, the presence of large complex spines on proximal dendrites and small, simple spines on distal dendrites underpins this resemblance. However, major differences in their morphology, connectivity, and physiological properties demonstrate that mossy cells constitute a discrete cell population (Amaral 1978; Buckmaster et al. 1993; Scharfman 2016).

The somata of the cells are slightly larger than those of CA3 pyramidal cells and have a triangular or ovoid shape. Three to six primary dendrites arise from the soma and bifurcate repeatedly to produce an extensive multipolar dendritic arborization confined to the hilus. Dendrites very rarely invade the granule cell layer or the molecular layer in mature rats (Amaral 1978; Ribak et al. 1985; Buckmaster et al. 1993; Lübke et al. 1998; but see Scharfman 1991). In vitro labeled mossy cells from mice have a total dendritic length of 5392 ± 313 μm (Kowalski et al. 2010), whereas in vivo labeled mossy cells from rats disclose a total dendritic length of 8293± 361 μm (adapted from Buckmaster 2012). Although these values are not directly comparable to those obtained for other types of hippocampal neurons, the extent of mossy cell dendritic arbor appears to lie between GCs and pyramidal cells.

Similarly, only limited quantitative data are available on synaptic inputs to mossy cells. Proximal dendrites and the soma are covered by complex spines reflecting a high degree of convergence of GC inputs onto electrotonically proximal locations (Frotscher et al. 1991; Acsády et al. 1998). Additionally, mossy fibers make synaptic contact with distal, simple dendritic spines (Frotscher et al. 1991). Other excitatory inputs include the hilar collaterals of CA3 pyramidal cells (Scharfman 1994, 2007; Jinde et al. 2013) and mossy cell axons terminating mainly on distal spines. However, data from paired intracellular recordings indicate that the mutual connectivity between mossy cells is very low (∼0.5%; Larimer and Strowbridge 2008). The major source of inhibitory input is from hilar interneurons (Acsády et al. 2000; Larimer and Strowbridge 2008).

The axon of mossy cells forms an extensive arbor in the ipsi- and contralateral hippocampi (Soltész et al. 1993; Buckmaster et al. 1996). While the extent of the dendrites is restricted along the septotemporal axis (<500 μm), the axon can cover 53–61% of the hippocampus (Buckmaster et al. 1996). Thus, mossy cells provide a distributed excitatory feedback to the DG. The ipsilateral length of the axon is between 73 and 96 mm (uncorrected two-dimensional projection, Buckmaster et al. 1996). Most of the axon is in the inner molecular layer (53–56%) and the hilus (23–27%), but collaterals are also found in the granule cell layer, the middle molecular layer, the CA3, and occasionally also the CA1 (Buckmaster et al. 1996). In the molecular layer, the axon forms synapses every ∼2 μm and the large majority of the postsynaptic targets are dendritic spines of GCs (Buckmaster et al. 1996). While numerically low, synaptic contacts onto interneurons have been suggested to play an important role in regulating the excitability of the DG (Ratzliff et al. 2002; Sloviter et al. 2003). In the hilus, interestingly, the density of synapses is five times lower along the axon (0.1 μm^{-1}), and the main targets are smooth dendrites of interneurons (Buckmaster et al. 1996; Larimer and Strowbridge 2008).

GABAergic Interneurons

Morphological Classification of Interneurons

Local inhibitory interneurons are characterized by extensive local axonal arborizations and can thereby provide inhibitory innervation and control the activity of large sets of local neurons. In contrast to the largely uniform population of principal cells, interneurons are extremely heterogeneous with respect to not only their morphological features but also their physiological characteristics and their expression of neurochemical markers and transcription factors. Differences in their properties are thought to reflect the functional diversity of interneurons in the network (Table 7). A key determinant of interneuron types is their origin, i.e., in which ganglionic eminence (either medial or caudal) are the cells formed during early embryonic development. Indeed, unique genetic markers define interneuron type, origin, and fate and their final location within the cerebral cortex (Kepecs and Fishell 2014). The most distinct anatomical feature of interneurons is the layer-specific distribution of their axon (Fig. 6). Correlated light and electron microscopic studies revealed that the axon projection reflects the differential targeting of subcellular compartments (e.g., soma, proximal, or distal dendrites) of the postsynaptic neurons (Han et al. 1993; Gulyás et al. 1993a; Buhl et al. 1994a). Additionally, termination of the axon often parallels afferent pathways leading to co-alignment of excitatory and inhibitory inputs.

However, not only the axon but also dendrites and cell bodies of interneurons show variability in their laminar distribution. While some interneuron types have a dendritic arbor spanning all layers, others have dendrites restricted to one or more layers. The dendritic distribution determines what inputs are available to an interneuron: whether it can be activated by one or more afferent system in a feedforward manner or by recurrent collaterals of principal cells as part of feedback inhibitory microcircuit (Fig. 6).

Thus, the precise localization of the interneurons, their dendrites, and axon within the layered structure of the hippocampus determines their anatomical connectivity. In turn, input and output connections define the functions that the cells can play in the circuitry. Therefore, most classification schemes have considered these anatomical features as defining criteria (Freund and Buzsáki 1996; McBain and Fisahn 2001; Somogyi and Klausberger 2005). Although there is still some debate regarding the terminology and identification of interneuron types (Maccaferri and Lacaille 2003; Petilla Interneuron Nomenclature Group et al. 2008), two main classes of interneurons can be distinguished on the basis of postsynaptic targets: perisomatic and dendritic inhibitory cells (Fig. 6). In addition, a set of interneurons that selectively target other interneurons (interneuron-specific [IS] cells; Acsády et al. 1996a, b; Gulyás et al. 1996; Hájos et al. 1996) and interneurons with long-range projections have been identified (Jinno et al. 2007; Melzer et al. 2012; Katona et al. 2017).

Table 7 Passive membrane parameters of the hippocampal principal cells and interneurons in morphologically and electrophysiologically constrained models

	*R*i (Ω cm)	*R*m (kΩ.cm^2)	*C*m (μF.cm^{-2})	Surface (1000 μm^2)	Reference
CA1 PC[a]	199	85.1	0.7	64.4	Major et al. (1993)
CA1 PC	228 (198–261)	27.2(16.1–39.9)	1.43(1.02–1.86)	42.8	Golding et al. (2005)[f]
CA1 PC	107 ± 10.7		170.1 ± 11.4 pF		Chevaleyre and Siegelbaum (2010)
CA2 PC	76.2 ± 11.1		305.3 ± 20.8 pF		Chevaleyre and Siegelbaum (2010)
CA3 PC	270 (170–340)	170(150–200)	0.75(0.69–0.81)	82.5 ± 5.2	Major et al. (1994)
CA3 PC	200/100[c]	50/1[c]	0.75	54.91	Traub et al. (1994)
CA3 PC	107.5 ± 28.1		150.1 ± 26.1 pF		Chevaleyre and Siegelbaum (2010)
GC	194 ± 24	38.0 ± 2.3	1.01 ± 0.03	13.3 ± 0.9	Schmidt-Hieber et al. (2007)
CA1 BC	296 ± 75	66.2 ± 37.8	1[e]	7.9 ± 0.9	Thurbon et al. (1994)
CA3 INs[b]	189 ± 130	62 ± 34	0.92 ± 0.34		Chitwood et al. (1999)
DG BC	121 ± 21	6.3/30.5[d]	1.1 ± 0.1	9.8/31.2[c]	Nörenberg et al. (2010)[f]

Abbreviations: *PC* pyramidal cell, *IN* interneuron, *Ri* axial resistivity, *Rm* membrane resistivity, *Cm* specific membrane capacitance

[a]Recordings were obtained with sharp microelectrodes and the simulations included a shunt to reproduce the leakage around the electrode

[b]The sample includes various interneuron types

[c]Values indicate somatodendritic/axonal compartments separately

[d]R_m before and after blocking Ih by ZD7288

[e]C_m was set as a constant

[f]Parameters of uniform models. For non-uniform models see original publications

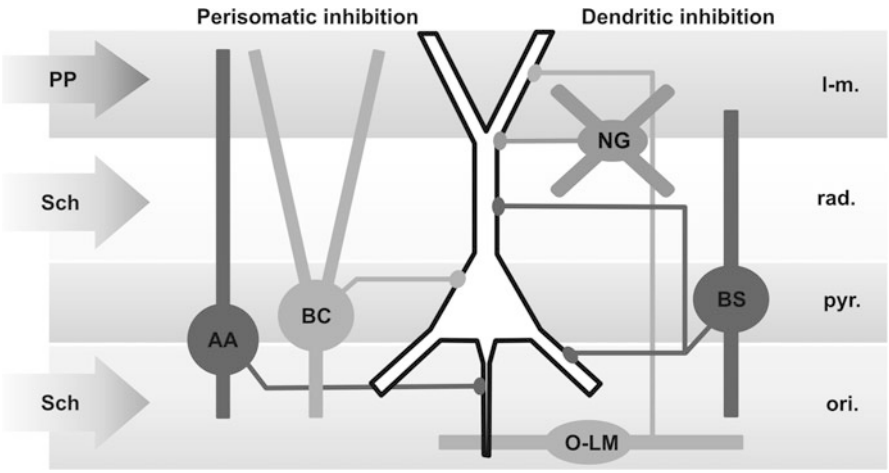

Fig. 6 Schematic representation of major interneuron types of the hippocampal CA1 area. Two main classes can be distinguished on the basis of postsynaptic targets: (1) *perisomatic inhibitory interneurons* include basket cells (BC, targets: soma and proximal dendrites) and axo-axonic cells (AA, targets: axon initial segments). The axon of these interneurons terminates in and near the str. pyramidale (pyr.). (2) *Dendrite-inhibiting interneurons* include many types. Here three well-characterized types are illustrated: (i) bistratified cells (BS) innervate the mid-distal dendrites in the *str. radiatum* (*rad.*) and *oriens* (*ori.*). (ii) Neurogliaform (NG) interneurons are found in the *rad.* or *str. lacunosum-moleculare* (*l-m.*) and inhibit the apical dendrites in the same layers. NG cells are mainly activated by the perforant path (PP) and the Schaffer collaterals (Sch) and therefore provide feedforward inhibition. (iii) O-LM interneurons are found in the *ori.* and innervate the distal apical dendrites in the *l-m*. O-LM cells receive strong recurrent excitation from pyramidal cells and therefore mediate primarily feedback inhibition

Perisomatic inhibitory interneurons innervate soma, proximal dendrites, and axon initial segments of principal cells. They include basket cells (BC) and axo-axonic cells (AAC, also known as *chandelier cells*). The majority of these cells has a vertically oriented dendritic tree and can mediate both feedforward and feedback inhibition.

Dendrite-inhibiting interneurons comprise several distinct types (Fig. 6) which innervate various portions of the dendritic tree of their target cells. The axon of dendrite-inhibiting interneurons is often co-aligned with afferent pathways in the dendritic layers (Han et al. 1993; Gulyás et al. 1993a; Vida et al. 1998; Vida and Frotscher 2000; Booker et al. 2017b). Thus, the various interneuron types can control excitatory postsynaptic responses in an input-specific manner (Miles et al. 1996; Maccaferri and Dingledine 2002). Furthermore, the co-alignment enables mutual presynaptic interactions between glutamatergic and GABAergic axons (Vogt and Nicoll 1999; Guetg et al. 2009; Min et al. 1999; Stafford et al. 2009; Urban-Ciecko et al. 2015). While some dendrite-inhibiting interneurons have dendrites spanning all layers and therefore can mediate feedforward and feedback inhibition, the majority of these cells have dendrites restricted to one or two layers. Interneurons

in the *str. oriens* and the hilus, such as O-LM interneurons, receive over 90% of their excitation from local principal cells and mediate feedback inhibition. In contrast, interneurons in the *str. radiatum* and *lacunosum-moleculare* are activated by the Schaffer collaterals and/or the perforant path and thereby mediate feedforward inhibition.

Neurochemical Classification of Interneurons

Interneuron types differentially express a wide range of molecular markers, including calcium-binding proteins (parvalbumin, PV; calbindin, CB; and calretinin, CR), neuropeptides (somatostatin, SOM; cholecystokinin, CCK; neuropeptide Y, NPY; vasoactive intestinal peptide, VIP), and certain enzymes (NADPH-diaphorase; neuronal nitric oxide synthase, nNOS). While the function of the molecules in these cells is not yet fully understood, detection of the markers by immunocytochemistry, in situ hybridization, single-cell RT-PCR, or RNA-seq investigations have been successfully applied to identify and classify GABAergic neurons (for reviews see Freund and Buzsáki 1996; Somogyi and Klausberger 2005; Jinno and Kosaka 2006; Houser 2007; Klausberger and Somogyi 2008; Pelkey et al. 2017). Importantly, the interneuron types defined on the basis of neurochemical identification converge well with the morphological classification, when the combinatorial expression pattern of multiple markers is considered (Table 8).

Interneurons of the CA1–3 Areas

Most interneuron types can be identified in all areas of the hippocampus on the basis of their salient anatomical properties. However, due to differences in the layering of the areas, some types may differ in certain anatomical properties, whereas a few specific types may exist only in one area. As the structure and layering of the CA1–CA3 areas are almost identical, we discuss interneuron types from these areas together. The classification and descriptions are based on results from the CA1 as this is the best study region of the hippocampus and possibly the whole cortex. But published data from the CA3 (Gulyás et al. 1993a) and the CA2 areas (Mercer et al. 2007; Botcher et al. 2014) confirm that the classification, with some exceptions, can be extrapolated to these regions.

Perisomatic Inhibitory Interneurons

(1) *Fast-spiking parvalbumin-positive basket cells.* PV-BCs form synapses with the somata and proximal dendrites of pyramidal cells as well as other interneurons (Buhl et al. 1994a; Halasy et al. 1996; Cobb et al. 1997; Pawelzik et al. 2002). At the light microscopic level, this interneuron type is characterized by an axon terminating in

Table 8 Divergence of neurochemical markers of hippocampal interneurons

	PV	CB	CR	SOM	CCK	VIP	NPY	CRH	NADPH	nNOS	GABAAα1	CoupTFII	Kv3.1b	Reelin	ErbB4	vGluT3	nAChR4α	mGluR1α	M2	μOR	CB1R	NR2D
Perisomatic inhibitory interneurons																						
PV-BC	++			+/−					++		++		++		++				++	++		++
CCK-BC		+/−			+++	+/−									++	+					++	
PV-AAC	++																		++	++		
Dendritic inhibitory interneurons																						
Bistratified cell	++			+			+												++	++		++
SCA		+			++										++	+/−					++	
PPA		+			++										++	+/−						
LA		?			++										++	+/−					++	
Neurogliaform							++			++	++	++		++						++		
Ivy cell							++			++	++	++								++		
O-LM/HIPP	+			++			+										++	++				++
MFA		++			++																	
Interneuron-specific interneurons																						
IS-I			++			+/−									++							
IS-II			+/−			++	++								++							
IS-III			+			++									++			++				
Long-range projecting interneurons																						
Back-projecting		+		++					++	++								++				
CRH		+	+	+				++														
Double/projection		+		++			+											++	+			

(++) indicates consistent high expression of the marker, (+) indicates low expression and/or expression in a subset, (−) indicates the consistent absence of the marker, when important for distinguishing types. For abbreviations, please see the text

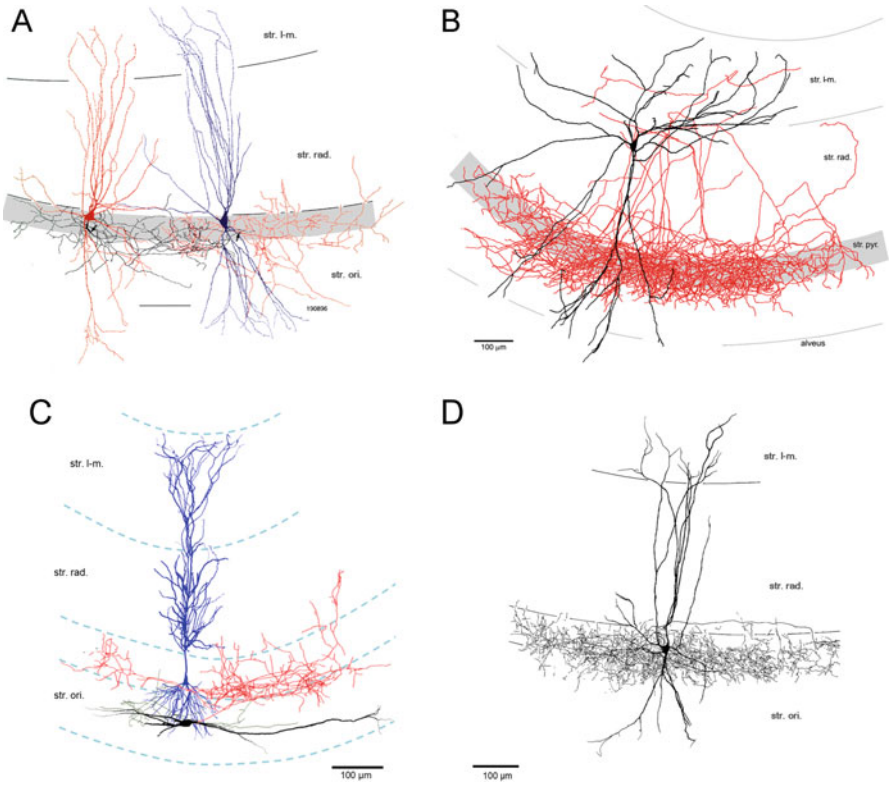

Fig. 7 Morphology of CA1 perisomatic inhibitory interneurons. (**a**) A synaptically coupled fast-spiking putative PV-positive BC-BC pair. The axons of both cells are found mainly in the cell body layer (shaded area, initial segments indicated by *arrows*), whereas their dendrites extend into the dendritic layers. (**b**) A BC with morphological feature of CCK-BCs with soma in the *str. radiatum* (rad.). Note the dense axon (*red*) in and near the cell body layer (str. pyr.). (**c**) A horizontal PV-BC with horizontally oriented dendrites restricted to the *str. oriens* (ori.) but with a typical BC axon arbor in the cell body layer. (**d**) An AAC with a dense axon plexus at the border of the *str. pyr.* and *ori*. Scale bars: 100 μm. (Reproduced with permission: (**a**) from Cobb et al. 1997, © Elsevier; (**b**) from Vida et al. 1998, © Wiley-Blackwell; (**c**), from Booker et al. 2017b, © The authors; (**d**) from Buhl et al. 1994b, © The American Physiological Society)

and near the cell body layer (Fig. 7a). In addition to PV, the cells express high levels of the alpha-1 subunit of $GABA_A$ receptors ($GABA_A$-α1; Table 8) as well as both $GABA_B$ receptor subunits ($GABA_{B1/2}$) and their effector Kir3 channels (Booker et al. 2013). It is estimated that PV-BCs constitute ~60% of all PV-immunoreactive cells and ~12% of all GABAergic interneurons in the CA1 area (Kosaka et al. 1987; Baude et al. 2007).

Cell bodies of PV-BCs are located in the *str. pyramidale* or *oriens*, but a few cells have been found in the *str. radiatum*. The dendrites are radially orientated and span all layers (Buhl et al. 1995, 1996; Halasy et al. 1996). Work published by

Gulyás et al. (1999) analyzed the distribution of dendrites and input synapses of PV-immunoreactive neurons. Although they could not unequivocally identify the cells as BCs, their results conceivably reflect characteristics of this predominant cell type. Their quantitative data revealed that the total length of the dendrites (4348 μm) is substantially shorter than that of pyramidal cells, but their laminar distribution is similar (Table 9). CA2 appears to be the anomaly for PV interneuron dendrites, with both narrow and wide dendritic arbors observed (312 ± 121 μm vs. 570 ± 111 μm lateral spread; Botcher et al. 2014).

The estimated total number of synapses (16,293, Table 9) is also markedly lower than for pyramidal cells, but it is the highest among interneurons (Gulyás et al. 1999); however their synaptic density is considerably higher. The proportion of excitatory (~93.5%) and inhibitory synapses (~6.5%) is comparable to that for pyramidal cells. As the dendrites of BCs lack spines, both excitatory and inhibitory synapses are formed onto dendritic shafts. Inhibitory synapses show a concentration in the perisomatic domain with ~17% of the synapses converging onto the soma, but in contrast to principal cells, the soma also receives a high number of excitatory synapses (Table 9). A large proportion of the inhibitory synapses are PV-immunopositive: ~27.6% on the dendrites and ~70% on the soma (Gulyás et al. 1999; Table 9). Thus, PV-containing interneurons are heavily interconnected by mutual inhibitory synapses (Sík et al. 1995; Fukuda and Kosaka 2000; Bartos et al. 2001, 2002). In addition to the chemical synapses, PV-BCs are also coupled by electric synapses to other PV-containing interneurons (Fukuda and Kosaka 2000, 2003; Bartos et al. 2001; Hormuzdi et al. 2001). Gap junctions are found primarily at dendritic locations with the highest density between basal dendrites at the *str. oriens*-alveus border (Fukuda and Kosaka 2000, 2003). This dual – chemical and electric – connectivity is thought to be important for the synchronization of the interneurons during network activity patterns, such as gamma oscillations (Bartos et al. 2001; Hormuzdi et al. 2001).

The output of BCs has been analyzed in both in vitro and in vivo labeled neurons. The length of the axon of in vivo-labeled BCs ranges between 40.5 and 53.5 mm and terminates in an approximately circular or ellipsoid area of the cell body layer with a diameter between 0.9 and 1.2 mm. It is emerging that BCs in the hippocampus exist with either narrow or wide axonal arbors; in the CA2 region, wide arbor BCs have axon spanning 937 ± 133 μm, whereas narrow arbor BCs span 616 ± 130 μm, suggesting that CA2 BCs project into both CA1 and CA2, suggesting a level of innervation of CA1 and CA3. This phenotype does not appear to exist within CA1 BC populations (Mercer et al. 2007). On the basis of the bouton density of 0.226 ± 0.039 μm^{-1}, the number of total synapses was estimated to be between 9000 and 12,000 (Sík et al. 1995). As unitary IPSCs in pyramidal cells are mediated by multiple, 10–12 synaptic contacts (Buhl et al. 1994a), the number of postsynaptic neurons (*divergence*) is likely to be between 750 and 1200 (Bezaire and Soltész 2013), whereas the number of PV-BCs making synaptic contacts onto a single postsynaptic pyramidal cell (*convergence*) is between 15 and 25 (Bezaire and Soltész 2013), calculated from the total number of synaptic contacts (92–119, Megías et al. 2001; Buhl et al. 1994a) and the number of contacts formed by a single

Table 9 Dendritic length and synaptic inputs of PV-containing interneurons of the CA1 area

			Density of synapses			Estimated number of synapses		
	Dendritic length (μm)	% of dendrites	All	Exc.	Inh.	Exc.	Inh.	PV+
Dendrites	4348 ± 1125					14,825	868	240
L-M	656 ± 255	(15.0%)						
Med	214 ± 124	(4.9%)	171.34	143.44	27.89			
Thin	442 ± 208	(10.1%)	155.72	126.75	28.97			
Rad	2369 ± 786	(54.5%)						
Thick	255 ± 165	(5.8%)	483.81	444.68	39.13			
Med	1713 ± 635	(39.4%)	432.68	416.01	16.67			
Thin	401 ± 219	(9.2%)	145.63	133.50	12.14			
Pyr	248 ± 121	(5.7%)						
Ori	1075 ± 535	(24.7%)						
Thick	21 ± 47	(0.4%)	612.94	568.45	44.49			
Med	686 ± 303	(15.7%)	361.08	344.95	16.13			
Thin	368 ± 243	(8.5%)	348.54	325.08	23.46			
Soma	1006 ± 184 μm^2 (surface area)					413	177	124
AIS						0	10	0
Total						15,238	1055	364

Values are mean ± S.E.M. Percentage values in parentheses indicate the proportion of dendrites within a layer. Density of synapses is per 100 μm. Excitatory (Exc.) and inhibitory (Inhib.) synapses were identified on the basis of postembedding immunolabeling for GABA. Data from Gulyás et al. (1999)

BC onto the soma (5–6, Gulyás et al. 1993a; Buhl et al. 1994a). Examples of PV-BCs with horizontal dendrites exclusively in *str. oriens* have also been described, suggesting divergent dendritic morphologies (Booker et al. 2017a, b; Fig. 7c)

(2) *CCK-expressing basket cells.* Similar to PV-BCs, CCK-BCs form synapses with the somata and proximal dendrites of pyramidal cells as also indicated by the axonal distribution in the *str. pyramidale* and adjacent region of *str. radiatum* and *oriens* (Fig. 7b; Nunzi et al. 1985; Acsády et al. 1996b; Cope et al. 2002; Pawelzik et al. 2002). In addition to CCK, neurochemical markers include VIP, substance P receptor, and vesicular glutamate transporter 3 (VGluT3), but the cells are consistently immunonegative for PV (Table 8; Cope et al. 2002; Pawelzik et al. 2002; Mátyás et al. 2004; Somogyi et al. 2004; Klausberger et al. 2005). Terminals of these interneurons express high levels of cannabinoid CB1 receptor which plays a role in regulating the release of GABA (Katona et al. 1999b). CCK-BCs mostly show regular-spiking discharge pattern, with some exceptions showing a fast-spiking phenotype (Cope et al. 2002; Pawelzik et al. 2002). In contrast to PV-BCs, cell bodies of CCK-BCs can be found in all hippocampal layers. The dendrites run radially and span all layers (Cope et al. 2002; Pawelzik et al. 2002). Mátyás et al. (2004) and Booker et al. (2017a, b) performed a detailed quantitative analysis of the laminar distribution of dendrites and input synapses of CCK-BCs. These analyses show that the total dendritic length of 6338 μm is higher than PV-BCs but markedly lower than pyramidal cells (Table 10). Despite the larger dendritic tree, the estimated total number of afferent synaptic contacts (8147, Table 10) is lower than for PV-BCs. This is due to the fact that the number of excitatory synapses is markedly lower. In contrast, the number of inhibitory synapses is ∼2.6-fold higher (Gulyás et al. 1999; Mátyás et al. 2004). Thus, CCK-BCs have a lower proportion of excitatory (∼64%) and a higher proportion of inhibitory synapses (∼36%) than both PV-BC and pyramidal cells. CCK-BCs are also interconnected by mutual inhibitory synapses. The number of CCK-immunopositive terminals on their surface is ∼350 (Table 10), very close to the number of mutual inhibitory synaptic contacts on PV-BCs. However, the proportion of these synapses among the inhibitory terminals is lower due to the higher overall inhibitory input (Mátyás et al. 2004). Although the PV- and CCK-interneuron networks seem largely independent, there is evidence for the existence of mutual inhibitory synapses and interactions between the two networks (Karson et al. 2009).

While immunocytochemical data at the light and electron microscopic levels demonstrate that terminals of CCK-BCs innervate soma and proximal dendrites of principal cells with a preference proximal to the soma (Földy et al. 2010; Nunzi et al. 1985; Acsády et al. 1996b; Cope et al. 2002; Pawelzik et al. 2002; Klausberger et al. 2005; Booker et al. 2017b), only limited data are available on the divergence or convergence of CCK-BC output. Bezaire and Soltész (2013) postulated a divergence of 1250 cells (1150 pyramidal cells and 100 interneurons) with a convergence of 13 CCK-BCs onto a single pyramidal cell.

(3) *Axo-axonic cells.* AACs provide GABAergic innervation to the axon initial segments of principal cells (Somogyi et al. 1983; Li et al. 1992; Gulyás et al. 1993a; Buhl et al. 1994a), placing them in a unique position to control action potential

Table 10 Dendritic length and synaptic inputs of CCK-BCs of the CA1 area

			Estimated number of synapses		
CCK +	Dendritic length (μm)	All	Excitatory	Inhibitory	CCK+
Dendrites	6338 ± 986	7948 ± 1229	5191 ± 805	2757 ±430	315 ± 55
L-M	1291 ± 456 (20.4%)	1876		759	
Rad/LM	647 ± 575 (10.2%)	798		258	
Rad	2876 ± 211 (45.4%)	3421		1074	
Pyr	111 ± 61	435		271	
Ori	311 ± 118 (4.90%)	1418			
Soma	966 ± 134 (surface area, μm^2)	193 ± 43	34 ± 14	5 ± 2	36 ± 14
AIS		6 ± 2	1 ± 1	5 ± 2	1 ± 2
Total		8147	5266	2921	352

Values are mean ± S.E.M. Values in parentheses indicate percentage of dendrites in a layer. Rad/L-M denotes the broader region of the two layers which contains many horizontally running dendrites. Excitatory (Exc.) and inhibitory (Inhib.) synapses were identified on the basis of postembedding immunolabeling for GABA. Data from Mátyás et al. (2004)

output of the target neurons. Similar to PV-BCs, the termination zone of the axon is mainly in the cell body layer, but it is slightly shifted toward the *str. oriens* (Fig. 7d). Many, but not all, AACs can be distinguished from BCs at the light microscopic level by the presence of vertical rows of synaptic boutons (cartridges), which form contacts with the axon initial segment (AIS). AACs show a fast-spiking discharge pattern and contain high levels of PV, but, in contrast to PV-BCs, they express low level of GABAA-α1 (Katsumaru et al. 1988; Pawelzik et al. 2002). It is estimated that this type constitutes ∼15% of all PV-immunoreactive cells and ∼3% of GABAergic interneurons in the CA1 area (Baude et al. 2007).

Cell bodies of AACs are located in the *str. pyramidale* or *oriens*. The majority has vertically oriented dendrites spanning all layers. In comparison with PV-BCs, the distal apical dendrites often branch and form an extensive tuft in the str. lacunosum-moleculare (Buhl et al. 1994b; Klausberger et al. 2003) indicating a stronger perforant path input to these neurons. A few cells with horizontally oriented dendrites in str. oriens have also been reported (Ganter et al. 2004).

AACs receive input from all major afferent pathways and there is also evidence for recurrent excitatory inputs from pyramidal cells (Li et al. 1992; Buhl et al. 1994b). Regarding the quantitative distribution of input synapses, Gulyás et al. (1999) suggested that their data may apply not only to PV-BCs but also to AACs (see Table 9). However, some disagreement remains regarding the extent of dendrites in the str. lacunosum-moleculare (see above). AACs are thought to be involved in the PV interneuron network coupled by gap junction and also receive inhibitory synapses from this network (Fukuda and Kosaka 2000; Baude et al. 2007). However, AACs themselves do not contribute inhibitory synapses to this network.

The output of AACs is directed exclusively to the AIS of principal cells (Somogyi et al. 1983). The synapses formed onto the AIS can contact the shaft directly or onto membrane protrusions that can receive 1–5 inhibitory synapses, with 25–130

AAC synapses formed per AIS (Kosaka 1980). Morphological analysis of an in vivo labeled CA1 AAC revealed that it can innervate ~1200 pyramidal cells within an area of 600 by 850 μm around the cell (Li et al. 1992). However, in vitro studies indicate that the axon can have a larger extent with values up to 950 μm in the CA1 and 1300 μm in the CA3 area (Gulyás et al. 1993a; Buhl et al. 1994b). The in vivo data further show that the cells form 2–10 synaptic contacts on a single axon initial segment (Li et al. 1992). As the number of synaptic contacts on initial segments is ~24 (Gulyás et al. 1999), 3–12 AACs may converge onto a single pyramidal cell (Bezaire and Soltész 2013).

Dendritic Inhibitory Interneurons

(4) *Bistratified cells (BSC)*. These interneurons are characterized by an axon in the *str. radiatum* and *oriens* co-aligned with the Schaffer collateral pathway (Fig. 8a; Buhl et al. 1994a, 1996). BSCs show a fast-spiking discharge pattern. They contain PV, the neuropeptides SOM, NPY, and high levels of the GABAA-α1 (Pawelzik et al. 2002; Klausberger et al. 2004; Baude et al. 2007). This type constitutes ~25% of all PV-immunopositive cells and ~5% of GABAergic interneurons in the CA1 area (Baude et al. 2007).

Cell bodies of BSCs, similar to other PV interneurons, are found primarily in the *str. pyramidale* or *oriens*. The dendrites show radial orientation and span *str. oriens* and *radiatum* but, in contrast to other PV interneurons, rarely invade the *str. lacunosum-moleculare* (Buhl et al. 1996; Halasy et al. 1996; Klausberger et al. 2004). A few cells with similar axonal arborization but horizontal dendrites have been reported and classified as oriens-BSCs (Maccaferri et al. 2000).

Dendritic distributions and electrophysiological data indicate that the cells are activated primarily by the Schaffer collaterals and can also receive recurrent excitatory input from pyramidal cells in the *str. oriens*, but they generally lack perforant path inputs (Buhl et al. 1996). It remains unclear whether the data on the quantitative distribution of synaptic inputs described for PV interneurons (Gulyás et al. 1999; see Table 9), apart from the lack of perforant path inputs, also apply to BSCs.

The output of BSCs targets shafts (~76–79%) and spines (~11–17%) of small-caliber dendrites and rarely the large-caliber main apical dendrites (~10%) or somata (~4%) of principal cells (Halasy et al. 1996; Klausberger et al. 2004). The proportion of interneuron targets is also low (~3%, Klausberger et al. 2004). Nevertheless, BSCs are thought to be involved in the network of PV interneurons connected by mutual inhibitory synapses and gap junction (Fukuda and Kosaka 2000; Baude et al. 2007). The axon of an in vivo labeled BSC has a total length of 78,800 μm and covers an area of 1860 μm (septotemporal) by 2090 μm (mediolateral axis). The axon of this cell has a bouton density of 0.21 ± 0.06 μm^{-1} and forms ~16,600 boutons. Since BSC-pyramidal cell synapses involve ~6 synaptic contacts (Buhl et al. 1994a), an individual BSC may target over 2500 pyramidal cells. A recent study, calculating 10 synaptic contacts made by a BSC

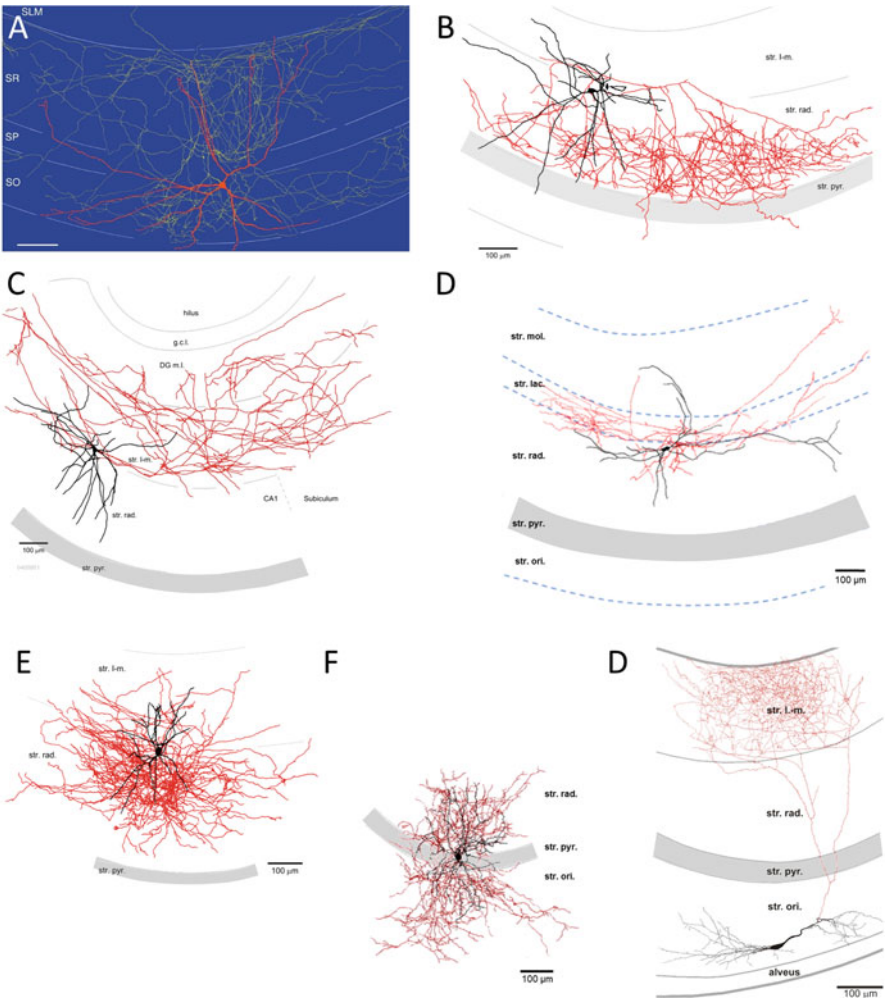

Fig. 8 Dendritic inhibitory interneuron types of the CA1 area. (**a**) A BSC with cell body at the border of *str. pyramidale* (SP) and *oriens* (SO). Dendrites span the str. radiatum (SR) and oriens, but do not extend into the *str. lacunosum-moleculare* (SLM). (**b**) SCA cell with axon (in *red*) in the *str. radiatum* (rad.). (**c**) PPA interneuron. Note the axon terminating in the CA1 *str. lacunosum-moleculare* (l-m.), the subiculum, and the DG molecular layer (m.l.). (**d**) A lacunosum-projecting (LA) interneuron, with axon and the majority of dendrites confined to *str. lacunosum* (lac). (**e**) NGF cell with a compact dendritic tree and a very dense axon in the *str. rad.* and *l-m*. (**f**) An Ivy cell with soma in *str. pyr*. and similarly dense focal axon around the soma. **G** O-LM interneurons have horizontal dendritic tree in the *str. oriens* (ori) and project to the distal apical dendrites of pyramidal cells in the *str. l-m*. (Reproduced with permission: (**a**) from Klausberger et al. 2004, © Nature Publishing Group; (**b, c, e)** from Vida et al. 1998, © Wiley-Blackwell; (**d**) from Booker et al. 2017b, © Oxford University Press; (**f**) from Krook-Magnuson et al. 2011, © The Society for Neuroscience**; G** from Martina et al. 2000, © The American Association for the Advancement of Science)

Table 11 Dendritic length and synaptic inputs of CB interneurons in the CA1 area Estimated number of synapses

	Dendritic length (μm)	All	Exc.	Inhib.
Dendrites	3441 ± 938	3585	2498 ± 666	1087 ± 277
L-M	130 ± 117 (3.8%)			
Rad	2622 ± 827 (76.2%)			
Pyr	197 ± 162 (5.7%)			
Ori	492 ± 300 (14.3%)			
Soma	799 ± 140 (surface area [μm^2])	244	102 ± 10	142 ± 15
AIS		7	0	7 ± 1
Total		3839	2601	1237

Values are mean ± S.E.M. Values in parentheses indicate percentage of dendrites in a layer. Excitatory (Exc.) and inhibitory (Inhib.) synapses were identified on the basis of postembedding immunolabeling for GABA. Data from Gulyás et al. (1999)

synapse, led to a convergence of 10 BSC onto a single pyramidal cell with a divergence to contact 1597 cells in total (Bezaire and Soltész 2013).

(5) *Schaffer collateral-associated (SCA) interneurons.* These interneurons, similar to BSCs, are characterized by an axon in the *str. radiatum* and *oriens* co-aligned with the Schaffer collaterals (Fig. 8b; Vida et al. 1998; Cope et al. 2002, Booker et al. 2017a). They differ, however, in their localization of the soma and dendrites, as well as neurochemical markers. The main markers are CCK and CB (Cope et al. 2002; Pawelzik et al. 2002; Klausberger 2009). Similar to CCK-BCs, SCA interneurons show a regular-spiking discharge pattern.

Somata of SCA cells are predominantly found in *str. radiatum*. Their dendrites run radially, mostly in the *str. radiatum*, but can extend into the str. *lacunosum-moleculare*, *oriens*, and even the alveus (Vida et al. 1998; Pawelzik et al. 2002; Booker et al. 2017a). Although dendritic arbor and synaptic inputs of identified SCA interneurons have not been quantitatively described, Gulyás et al. (1999) provide data on CB-immunoreactive interneurons, a set of dendritic inhibitory interneurons (Gulyás and Freund 1996) which overlap with the SCA type (Cope et al. 2002). The total dendritic length of CB interneurons is 3441 ±938 μm with 76% localized in the *str. radiatum* (Table 11). The excitatory input is relatively weak (~68%) and originates plausibly from the Schaffer collaterals, whereas the inhibitory input is strong (32%). Large part of the inhibitory input may correspond to the mutual inhibitory connections observed between CCK and SCA cells (Ali 2007). In addition to the chemical synapses, SCA cells have been shown to be connected by gap junctions (Ali 2007).

The axon of SCA cells terminates in the *str. radiatum* and to a lesser extent in the *str. oriens*. Output synapses are formed with shafts, but only rarely spines of small-caliber side branches of the pyramidal cells (~80%) and aspiny dendritic shafts of interneurons (~20%; Vida et al. 1998). Synaptic effects in pyramidal cells are mediated by multiple contacts (4–6, light microscopic estimates, Vida et al. 1998;

Pawelzik et al. 2002). The axon of an in vitro labeled SCA interneuron formed ~6000 boutons and may innervate 1000–1500 postsynaptic cells within a 400 μm slice.

(6) *Perforant path-associated (PPA) interneurons.* This cell type has an axon in the str. lacunosum-moleculare co-aligned with the perforant path (Fig. 8c; Vida et al. 1998; Pawelzik et al. 2002). Neurochemical markers of PPA cells include CCK (Pawelzik et al. 2002; Klausberger et al. 2005) and they may also express CB. Cell bodies of PPA cells are in the str. radiatum or lacunosum-moleculare, often at the border of the two layers. Dendrites run radially in these two layers but can also extend into the oriens/alveus (Hájos and Mody 1997; Vida et al. 1998). The dendritic distribution suggests that the cells' input is primarily from the perforant path and Schaffer collaterals, but they may also receive feedback excitation on their distal dendrites in the oriens/alveus.

The axon terminates in the str. lacunosum-moleculare; however, collaterals often spread significantly into the subiculum and, crossing the fissure, into the DG. The postsynaptic targets are primarily principal cells, CA1 pyramidal cells (58–94%), and DG granule cells (0–26%) but also include interneurons (6–11%); the synapses are found mostly on small-caliber dendritic shafts and to a lesser extent (5–7%) dendritic spines (Vida et al. 1998; Klausberger et al. 2005). This cell type provides a convergence of two PPA interneurons onto a single pyramidal cell and can diverge to 1333 neurons (Bezaire and Soltész 2013).

(7) *Lacunosum-associated (LA) cell.* This subtype of interneuron has only recently been described (Fig. 8d, Booker et al. 2017a) and represents a novel dendritic inhibitory subtype. With horizontal somata found in *str. lacunosum*, they have horizontally orientated dendrites and axons. Over 50% of LA cell axon is found within str. lacunosum itself, with dendrites confined to proximal *str. radiatum* and *moleculare.* Of the 5 neurons identified, all are CCK and CB1R immunoreactive and have unique electrophysiological properties (Booker et al. 2017a). The full physiological role of these neurons is yet to be ascertained, but their axonal plexus being found close to CA1 PC primary dendrite bifurcation points suggests a role in branch integration and/or calcium signaling.

(8) *Neurogliaform (NG) cell.* This interneuron type is identified on the basis of a small, stellate dendritic arbor and an extremely dense local axon (Fig. 8e, Vida et al. 1998; Price et al. 2005). NG cells express NPY, NOS, COUP TFII, α-actinin, and reelin as well as high levels of α_1 and δ and $GABA_A$ and μ-opioid receptors, but are consistently negative for PV (Price et al. 2005, Fuentealba et al. 2010; Tricoire et al. 2010; Armstrong et al. 2011, 2012; Krook-Magnuson et al. 2011; Table 8). However, there is a high heterogeneity from cell to cell in their marker expression (Armstrong et al. 2012). The small, round cell body is located in the *str. radiatum* or *lacunosum-moleculare;* within the DG their cell bodies are found at high density at the border with the hippocampal fissure (Armstrong et al. 2011). Several main dendrites emerge from the soma and branch profusely to form a very dense local dendritic arbor. There are no quantitative anatomical data on the input synapses of NG cells. Electrophysiological recordings indicate that the cells receive excitatory input from both the perforant path and the Schaffer collaterals (Price et al. 2005).

Inhibition is mediated by O-LM interneurons (Elfant et al. 2008) and other NGs cells through mutual inhibitory synapses with unique unitary synaptic properties (~70% connectivity, Price et al. 2005). The NG cells are also extensively coupled by gap junctions (~80% connectivity, Price et al. 2005).

The axon forms an extremely dense arbor in the *str. radiatum* and *lacunosum-moleculare* in the vicinity of the cell. An in vitro-labeled NG cell formed almost 13,000 boutons within its termination zone with less than 700 μm diameter along the transverse axis. Postsynaptic targets are mainly pyramidal cell dendritic shafts (~89%) but also spines (11%; Vida et al. 1998). Interestingly, unitary postsynaptic effects of NG-IPSCs are unusually slow and involve not only $GABA_A$ but also $GABA_B$ receptors (Tamás et al. 2003; Szabadics et al. 2007; Price et al. 2008). In fact, postsynaptic response mediated by both these receptor types is elicited in the absence of synaptic contacts through volume transmission plausibly due to the dense and focal axon and the presence of high-affinity extrasynaptic receptors (Szabadics et al. 2007; Oláh et al. 2009). Recent evidence suggests that NG cells in the DG are capable of forming multifarious synapses between both presubiculum, CA1 and the DG, as the axon of some NG cells profusely crosses the hippocampal fissure, with axon varicosities observed on these crossing axons (Armstrong et al. 2011).

(9) *"Ivy" interneurons.* Similar to NG cells, Ivy interneurons can be distinguished by a very dense axonal plexus close to the soma terminating in *str. oriens* and *radiatum* (Fig. 8f, Fuentealba et al. 2008). These cells are immunoreactive for NPY, NOS, COUP TFII, and α-actinin as well as express high levels of α_1 and δ and $GABA_A$ and μ-opioid receptors but are negative for reelin (Fuentealba et al. 2010; Tricoire et al. 2010; Armstrong et al. 2011, 2012; Krook-Magnuson et al. 2011; Table 8). They show a slow-spiking discharge pattern. Ivy cells are more numerous than PV-positive perisomatic inhibitory cells (~1.4-fold higher density, Fuentealba et al. 2008) and may comprise ~20% of all GABAergic interneurons.

Cells bodies of Ivy interneurons are located in the *str. pyramidale* and adjacent regions of the *radiatum*. Dendrites extend radially into the str. oriens and radiatum but rarely reach the str. lacunosum-moleculare. Dendritic distribution and electrophysiological data indicate that these interneurons are activated by the Schaffer collaterals and receive recurrent excitatory input from pyramidal cells, but lack perforant path input, similar to BSCs (Fuentealba et al. 2008).

Postsynaptic targets of Ivy cells are primarily the shafts (81%) of basal dendrites in str. oriens and oblique dendrites in the str. radiatum (Fuentealba et al. 2008). Dendritic spines (13%) and apical dendrites of pyramidal cells (6%) are less frequently targeted. The axon profusely branches close to its point of origin and forms a dense meshwork in the str. oriens and radiatum. In comparison with BSCs labeled under similar conditions, the area covered by axon collaterals is slightly smaller (Ivy, 0.75 ± 0.12 mm [mediolateral] by 1.31 ± 0.11 mm [rostrocaudal], Fuentealba et al. (2008); BSC, 1.15 ± 0.26 mm by 1.53 ± 0.38 mm, Klausberger et al. 2004). However, Ivy cells have a denser axonal plexus, especially in the str. oriens, and representative samples indicate an approximately two times higher total axon length (Fuentealba et al. 2008). Thus, Ivy cells could innervate larger sets

of postsynaptic neurons than BSCs. Indeed, a single Ivy cell can contact up to 1620 cells and on each pyramidal cell a total of 42 Ivy cells converge (Bezaire and Soltész 2013).

(10) *Oriens lacunosum-moleculare-projecting* (O-LM) *interneurons*, as their name indicates, are located in the str. oriens and project to the *str. lacunosum-moleculare* (Fig. 8g; McBain et al. 1994; Sík et al. 1995; Maccaferri et al. 2000). These interneurons are immunopositive for SOM, the metabotropic glutamate receptor mGluR1α, occasionally weakly positive for PV (∼50% of neurons; Booker et al. 2018; Table 8), NPY (Kosaka et al. 1988; Baude et al. 1993; Klausberger et al. 2003), and specifically in CA1 the nicotinic acetylcholine receptor α4 subunits (Leão et al. 2012). SOM interneurons constitute ∼14% of all GABAergic neurons in the hippocampus (Kosaka et al. 1988), but the exact proportion of O-LM cell subset has not yet been established. At the str. oriens/alveus border, approximately 95% of SOM interneurons are of O-LM type, with the remaining 5% being bistratified (Booker et al. 2018)

The soma of O-LM interneurons is located in the *str. oriens*, often at the border to the alveus. The dendritic tree has a horizontal orientation and is restricted to the *str. oriens* and the alveus. In contrast to most other interneurons, the dendrites are densely covered with long, thin spines. Electron microscopic investigations indicate that ∼20% of the afferent synaptic contacts are inhibitory and ∼80% excitatory (Blasco-Ibáñez and Freund 1995). Although the dendritic arbor falls in the termination zone of the Schaffer collateral pathway, degeneration studies revealed that over ∼75% of excitatory synapses originate from the pyramidal cells in the CA1 area (Blasco-Ibáñez and Freund 1995), with direct synaptic contacts being formed from local pyramidal cell (Lacaille et al. 1987). Thus, these interneurons primarily mediate feedback inhibition. CA1 O-LM cells themselves also receive a near homogeneous inhibitory input from CR-containing interneurons (70% of inputs; Tyan et al. 2014). In the CA3 area, the cell bodies and dendrites of this type of interneuron are not restricted to the *str. oriens*, in accordance with the wider distribution of recurrent collaterals seen in this region. A smaller set of interneurons with similar axonal projection and neurochemical profile but with somata located in the *str. pyramidale* (P-LM cells) or *radiatum* (R-LM cells) and dendrites spanning *str. radiatum* and *oriens* have been identified in transgenic "GIN" mice (Oliva Jr et al. 2000).

The axon of O-LM cells originates often from one of the main dendrites (Martina et al. 2000). Major collaterals ascend to the *str. lacunosum-moleculare* (often bifurcating within *str. radiatum)* and form a dense arborization in that layer. Some cells additionally form an axonal arbor, albeit much less extensive, in the *str. oriens*. The axon of an in vivo-labeled O-LM cell has a length of 63,436 μm occupying a relatively small termination field of 500 μm by 840 μm (mediolateral and septotemporal axes; Sík et al. 1995). Interestingly, in vitro-labeled O-LM interneurons in the CA3 show similar restricted axon projection in transverse slices but form multiple innervation fields along the septotemporal axis (Gloveli et al. 2005a). Over 91% of the collaterals are found in the *str. lacunosum-moleculare*, only 7% in the *str. oriens*, and a small proportion invading the subiculum. The

bouton density is $0.27 \pm 0.04\ \mu m^{-1}$ and the number of boutons was calculated to be over 16,800 (Sík et al. 1995). However, electron microscopic analysis of in vitro-labeled neurons showed that the axon can make synaptic contacts without forming varicosities, therefore it is difficult to estimate the total number of output synaptic contacts (Maccaferri et al. 2000). Postsynaptic targets of O-LM cells include dendrites of principal cells and interneurons in proportion to their occurrence (Katona et al. 1999a; Elfant et al. 2008). The synapses are found on dendritic shafts (~70%) and to a lesser degree on spines (~30%; Sík et al. 1995; Katona et al. 1999a; Maccaferri et al. 2000). Briefly, a single O-LM cell can innervate 1457 pyramidal cells and 180 interneurons and 8 O-LM cells converge onto a single principal cell (Bezaire and Soltész 2013).

(11) *Trilaminar (TL) interneurons*. This interneuron type is characterized by an axon distributed to three adjacent layers (hence the name): the *str. radiatum, pyramidale*, and the *oriens* (Sík et al. 1995; Gloveli et al. 2005b; Ferraguti et al. 2005). TL cells express high levels of muscarinic acetylcholine receptor (M2), but other markers are unknown (Hájos et al. 1998; Ferraguti et al. 2005).

The cells show some similarities to O-LM interneurons. Their cell bodies are located in the *str. oriens* and the dendritic trees are restricted to the same layer. The dendrites are sparsely spiny. The cells receive synaptic input from excitatory and inhibitory terminals expressing high levels of mGluR8, indicating a strong glutamatergic modulation of the input (Ferraguti et al. 2005). The cellular origin of the synapses is unknown, but local pyramidal cells are likely to be involved in the excitatory input. A part of the inhibitory terminals shows immunoreactivity for VIP and is likely to originate from a subset of IS interneurons (Ferraguti et al. 2005).

The axon terminates in the *str. radiatum, pyramidale, and oriens* and extends into neighboring areas, i.e., to the subiculum from the CA1 (Ferraguti et al. 2005) or the CA1 from the CA3 (Gloveli et al. 2005b) and may also project to other brain areas as well. The total axon length of an in vivo-labeled TL cell in the CA1 area was 55,913 μm and covers an area of 2600 μm (septotemporal) by 2450 μm (mediolateral) (Sík et al. 1995). Based on bouton density ($0.28 \pm 0.05\ \mu m^{-1}$), the calculated number of boutons is 15,767. Synapses formed by TL cells constitute 10 synaptic contact sites, and a single TL cell can innervate approximately 1544 cells (Bezaire and Soltész 2013). Postsynaptic neurons of TL cells locally include pyramidal cells and an unusually high proportion of interneurons. In the CA1, the targets are interneuron dendrites (44%), interneuron cell bodies (8%), pyramidal cell dendritic shafts (25%), and somata (23%; Ferraguti et al. 2005).

(12) *Mossy fiber-associated (MFA) interneurons.* This interneuron is a specific CA3 type and characterized by an axon plexus in the str. lucidum co-aligned with mossy fibers (Fig. 9; Vida and Frotscher 2000; Losonczy et al. 2004). MFA interneurons express CCK and high levels of CB1 receptor in their synaptic terminals maintaining a very low initial release probability (Losonczy et al. 2004). The small round or ovoid soma of MFA cells is located in or near the *str. lucidum*, and their dendrites extend radially into the str. radiatum and the oriens. The dendritic distribution indicates that the main sources of excitation are ipsi- and contralateral

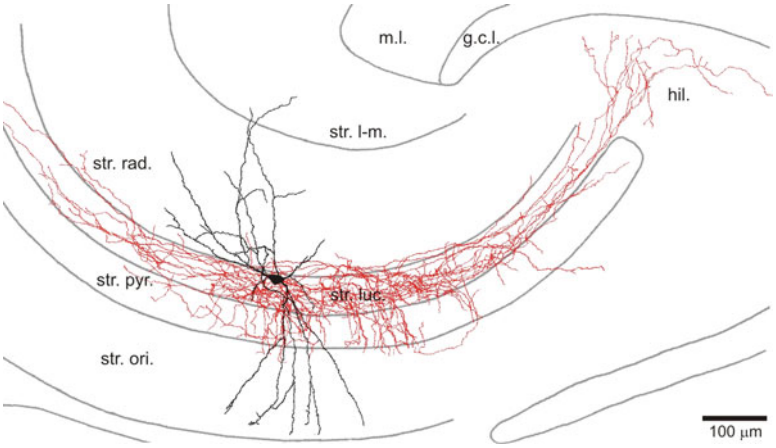

Fig. 9 MFA interneurons of the CA3 area. The axon (*red*) of this interneuron type terminates mainly in the str. lucidum (luc.) but also extends into the hilus displaying a striking association to the mossy fiber projection. The dendrites are found in the *str. radiatum* (rad.) and *oriens* (ori.) but absent from the *str. lacunosum-moleculare* (m-l.), reflecting that the cells receive excitatory input primarily from ipsi- and contralateral CA3 pyramidal cells. (Reproduced from Vida and Frotscher 2000 with permission. © National Academy of Sciences, USA)

CA3 pyramidal cells (i.e., the recurrent collaterals and commissural fibers), but physiological data (Tóth and McBain 1998) further show that the cells also receive mossy fiber input. No or minimal excitatory input arrives to these cells from the perforant path.

The axon forms a dense plexus in the str. lucidum, covering 50–100% of the transverse extent of the CA3 and fanning out into the hilus. Additionally, some collateral extend into the cell body layer. The axonal distribution is strikingly similar to that of the mossy fibers; this cell type best exemplifies the co-alignment of inhibitory interneuron axons and excitatory afferent pathway. Synaptic contacts are located on dendritic shafts (85%), mostly large-caliber proximal dendrites, and to a lesser degree on somata (15%) in the CA3 area. Majority of the targets are pyramidal cells, although ~20% of the postsynaptic profiles belong to GABA-immunoreactive interneurons (Vida and Frotscher 2000). The length of the axon in the in vitro-labeled neurons is 20.3–28.6 mm and forms ~5000–7000 boutons (density, 0.23 – 0.25 μm^{-1}). As the postsynaptic pyramidal cells are innervated by ~4 synaptic contact sites, a single MFA interneuron may target 1300–1700 neurons.

Interneuron-Specific Interneurons

A class of interneuron specialized to innervate other interneurons has been identified by imunohistochemically staining for CR and VIP (Acsády et al. 1996a, b; Gulyás

et al. 1996; Hájos et al. 1996; Table 8). Three types have been distinguished on the basis of the neurochemical markers and synaptic targets (Fig. 10):

(13) *Type I (IS-I) cells* contain CR, the soma of IS-I cells is in *str. oriens, pyramidale*, or *radiatum* and the dendrites span most layers (Acsády et al. 1996a; Gulyás et al. 1996). They target CB-positive dendrite-inhibiting interneurons but avoid PV-expressing BCs and axo-axonic cells. Furthermore, these interneurons form extensive mutual inhibitory connections as well as making dendrodendritic contacts coupled by gap junctions (Gulyás et al. 1996; Fig. 10).

(14) *Type II (IS-II) cells* express VIP and their soma is found in *str. radiatum*, often at its upper border, whereas the dendrites mostly extend into the *str. lacunosum-moleculare* and are densely spiny. These interneurons preferentially innervate CCK/VIP-positive basket cells. Furthermore, they form inhibitory synapses onto CR interneurons, thereby contributing to the mutual inhibitory network of IS-I cells, but receiving no output from this network.

(15) *Type III (IS-III) cells* contain both VIP and CR and have soma located in *str. pyramidale* or *radiatum* with radial dendrites, which show either unipolar or bipolar morphologies spanning most layers and forming a tuft in the str. L-M (Acsády et al. 1996b; Gulyás et al. 1996; Chamberland et al. 2010). IS-III have an axon mostly localized to *str. oriens* and mainly target SOM-positive interneurons in this layer, in particular O-LM cells, with a connection probability of 56%, which is higher than for BCs (10%) or BSCs (16%), but they never contacted CA1 PCs (Tyan et al. 2014). Interestingly, as their main targets, the O-LM cells, IS-IIIs also express mGluR1α on their somatodendritic domains (Ferraguti et al. 2004), and additionally mGluR7 are localized to their axon terminals (Somogyi et al. 2003).

INs with Local and Long-Range Projecting Axons

While interneurons are characterized by an extensive local axon restricted to a given area, it has long been noted that axon collaterals of some types, for example, those localized close to the fissure, such as CA1 PPA cells, crossed boundaries of the area and often extend into the neighboring area, e.g., the ML of the dentate gyrus (Vida et al. 1998). Additionally, interneurons were identified with major axon collaterals forming distinct collateralizations in other hippocampal areas. First and most prominent example was described by Sík et al. (1994) as BP cells found in the str. oriens of the CA1 area (see type 12 above). Finally, a subset of INs possesses both local and long-range projecting axons, targeting retrohippocampal regions or the septum. The latter two group of INs are referred to as projection INs and are believed to synchronize activity across brain regions, allowing coordinated neuronal firing.

(16) *Back-projection (BP) interneurons.* This interneuron type was named for its extensive axon projecting "back" to the CA3 area and the hilus from the CA1 (Sík et al. 1994, 1995). BP cells have been suggested to correspond to a subset of NADPH-diaphorase and NOS-immunoreactive cells (Sík et al. 1994) and were also found to express SOM and CB (Goldin et al. 2007; Gulyás et al. 2003; Table 8). The

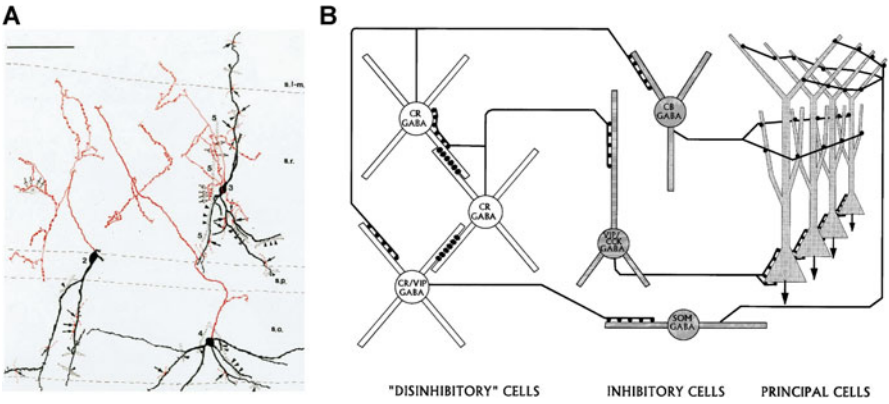

Fig. 10 IS interneurons of the hippocampus. (**a**) Camera lucida drawing of CR-containing interneurons of the CA1 area (cell bodies and dendrites are in black; axons are in *red*). The cells often form dendrodendritic and axodendritic contacts with each other. Synaptic partners are indicated by *dotted outlines*. Arrowheads indicate locations where the dendrites ran parallel in close contact. (**b**) Simplified schematic representation of hippocampal microcircuits including IS interneurons ("disinhibitory cells"). IS cells are interconnected by dendrodendritic (bars on dendrites) and axodendritic contacts which presumably serve their rhythmic and synchronized activity. The cells' output is directed to and controls the activity of several types of inhibitory interneurons including CCK- and VIP-containing BCs (VIP/CCK GABA), O-LM interneurons (SOM GABA), and CB-immunoreactive dendritic inhibitory interneurons (CB GABA). (Reproduced from Gulyás et al. 1996 with permission. © The Society for Neuroscience)

somatodendritic domain of BP cells is bipolar and confined to the *str. oriens* and shows similarities to other horizontal interneuron types of this layer (e.g., O-LM cells) including the presence of long, thin spines. The total length of axon collaterals is 20,642 μm, 59% of which is in the CA1 region and 41% project back to CA3 area innervating the *str. oriens* and *radiatum*. The synaptic connections of these cells have not been studied in detail, but they form synapses on dendrites and somata of pyramidal cells in the CA1 (Sík et al. 1994).

On the basis of their local axonal distribution, these cells may overlap with previously described oriens-BSC and/or TL cells identified morphologically in slice preparation. Furthermore, interneurons with long-range projection to the septum (*double-projections cells*; see below) have similar neurochemical profile and intrahippocampal projection pattern and may overlap, at least partially, with this interneuron type (Gulyás et al. 2003; Goldin et al. 2007).

(17) *Corticotropin-releasing hormone-expressing interneurons.* A recently described CA1 interneuron type, which selectively expresses corticotropin-releasing hormone (CRH) (Yan et al. 1998; Hooper and Maguire 2016). Found within the CA1 *str. pyramidale*, these neurons also express SOM (40% of neurons), CB (27% of neurons), and CR (23% of neurons) and may also express PV and CCK. They

have large ovoid somata and vertically oriented dendritic tree, spanning *str. oriens* and *radiatum,* reminiscent of CA1 PCs. Their axon projects to the *str. pyramidale* of CA3, providing strong inhibition to cell bodies of CA3 PCs (Hooper and Maguire 2016).

(18) *RADI cells* express CB and COUP-TFII and have somata in *str. L-M*, with short dendrites that remain in the same layer (Fuentealba et al. 2010). The axon of RADI cells densely innervates *str. radiatum*, forming synaptic contacts with the dendrites of CA1 PCs and other interneurons, but minimally ramifies in *str. L-M*. In addition, RADI cells send an axon collateral across the hippocampal fissure to *str. granulosum* of the DG, forming BC like synapses with the cell bodies of dentate granule cells (Fuentealba et al. 2010).

(19) *Double-projecting interneurons* are characterized by a long-range axonal projection to the septum and retrohippocampal areas, in addition to its intrahippocampal axon (Jinno et al. 2007; Fig. 11). Similar to many other interneuron types in the oriens/alveus, their somata and dendrites are located in *str. oriens* and they are immunoreactive for SOM, CB, NPY, and MGluR1α (Gulyás et al. 2003; Jinno et al. 2007). Interestingly, in the CA3 interneurons with hippocampo-septal projection also exist and mostly express SOM, but instead of CB they show CR immunoreactivity (Gulyás et al. 2003). In the CA1, they have horizontal

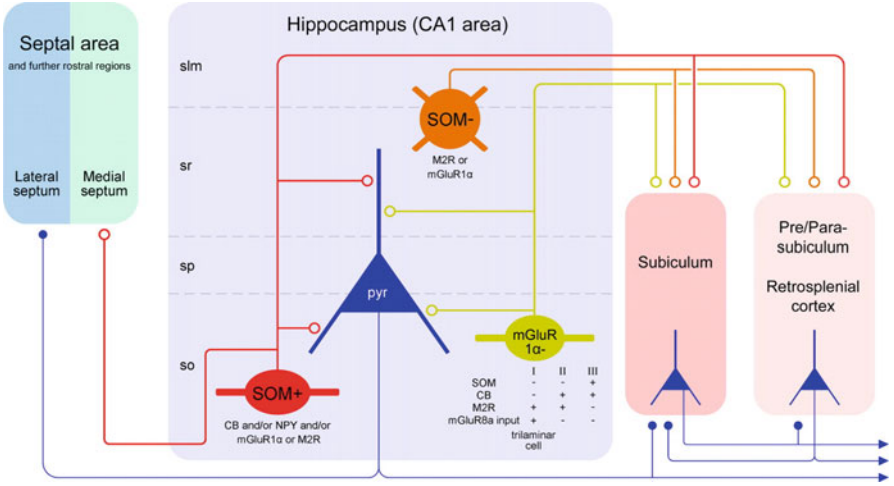

Fig. 11 Long-range projecting interneurons of the hippocampus. The schematic diagram shows the three main subsets of CA1 hippocampal GABAergic neurons projecting to the septal and/or retro-hippocampal areas. The first major population (double-projecting cells, in red) is located in str. oriens and projects to both the retrohippocampal and septal areas. The second population (*oriens/retrohippocampal projection cells, in* green) is less common in str. oriens, projects exclusively to the subicular areas, and shows diverse molecular expression profiles, as indicated below the cell. The third population (*radiatum/retrohippocampal projection cells,* in brown), found in the str. radiatum and lacunosum-moleculare, projects to retrohippocampal areas but not to the septum. (Reproduced from Jinno et al. 2007 with permission. © The Society for Neuroscience)

dendrites restricted to the *str. oriens*; however some multipolar and vertical examples have been observed. Double-projecting neurons have intrahippocampal axonal arborization in the CA3 and DG, in addition to their thick and strongly myelinated long-range retrohippocampal and a septal axon collaterals. The major divergence of double-projecting cells is with respect to their target cells. While some of these interneurons contact spiny principal cell dendrites (Jinno et al. 2007), others have been shown to preferentially contact interneuron dendrites (Gulyás et al. 2003). Therefore it remains ambiguous to what extent these cells are one class or multiple subtypes.

(20) *Oriens/retrohippocampal projection* cells have somata and bipolar, horizontal dendrites confined to *str. oriens,* comparable in morphology to other horizontally oriented *str. oriens/alveus* interneurons. These interneurons are immunoreactive for CB, as well as SOM. Oriens retrohippocampal projection INs possess a dense axon in *str. radiatum* and *oriens* of CA1, where they predominately contact CA1 PC dendrites (Jinno et al. 2007). The myelinated projection axon ramifies in either subiculum or the mEC where, in contrast to the local collaterals, it seems to preferentially form synapses onto INs (Melzer et al. 2012).

(21) *Radiatum/retrohippocampal projection* interneurons have soma located at the *str. radiatum/L-M* border region and radially oriented dendrites spanning these layers. *Their* axon which may form local synapses in the *str. L-M* sends a thick, myelinated axon to the subiculum, presubiculum, retrosplenial cortex, and indusium griseum, where it preferentially forms synapses with GABAergic interneurons dendrites.

Interneurons of the DG and Hilus

The layering of the DG differs markedly from that of the CA areas. Therefore, many of the DG interneuron types show differences in their morphology to their counterparts in those areas. In the following section, we briefly review the main morphological feature and connectivity, whenever known, of the major DG interneuron types.

Perisomatic Inhibitory Interneurons

(1) *Fast-spiking PV-BCs* are the best investigated interneuron type of the DG (Han et al. 1993; Halasy and Somogyi 1993b; Scharfman 1995; Sík et al. 1997; Mott et al. 1997; Bartos et al. 2001, 2002; Doischer et al. 2008; Nörenberg et al. 2010). The somatodendritic morphology is reminiscent of pyramidal cells. The large triangular or ovoid soma is located in the granule cell layer, often at the border to the hilus. Apical dendrites extend into the molecular layer and can receive input from all major afferent pathways. Basal dendrites are found in the hilus and receive recurrent excitatory input from mossy fibers mediated by multiple, 2–4 distributed contacts

(Geiger et al. 1997). The mean surface area of the apical and basal dendrites of in vitro labeled BCs is 7600 and 2200 μm^2, respectively (Nörenberg et al. 2010). The main postsynaptic targets of BCs are GCs (Geiger et al. 1997; Kraushaar and Jonas 2000; Bartos et al. 2002). Similar to the CA areas, DG PV-BCs are also extensively coupled by mutual inhibitory synapses (70–80% connectivity for closely spaced BCs) and gap junctions (~30% connectivity, Bartos et al. 2001, 2002).

(2) *CCK-BCs* were described in the in vivo labeling study by Sík et al. (1997), but no further data have been obtained from identified CCK-BC from the DG.

(3) *AACs* of DG were first described in detail by Han et al. (1993) and Buhl et al. (1994a, b). Somatodendritic morphology of AACs is largely similar to that of BCs. The output is directed exclusively to the axon initial segment of GCs. These synapses involve multiple contact sites; in case of one AAC-GC pair, eight contacts were identified and the number of AACs converging onto the same initial segment was calculated to be five (Buhl et al. 1994a).

Dendritic Inhibitory Interneurons

(4) *Molecular layer perforant path-associated (MOPP) interneurons* are located in the molecular layer and project to the outer two-thirds of this layer co-aligned with the perforant path (Han et al. 1993; Halasy and Somogyi 1993b; Sík et al. 1997). A subset of molecular layer interneurons shows a similar projection in the DG, but many of its axon collaterals cross the hilus and terminate in the CA1 area and/or the subiculum ("OML cells," Ceranik et al. 1997; Hosp et al. 2005). Many features of these interneurons correspond to those of CA1 PPA cells.

(5) *Hilar perforant path-associated (HIPP) interneurons* (Han et al. 1993; Halasy and Somogyi 1993b; Sík et al. 1997; Hosp et al. 2005) correspond to O-LM interneurons of the CA areas. Their soma and dendrites are confined to the hilus and receive recurrent excitation from the mossy fibers. Their axon terminates in the outer two-thirds of the molecular layer parallel to the perforant path. Thus, HIPP interneurons constitute the main feedback dendritic inhibitory cell types of the DG. Similar to O-LM cells, HIPP cells express SOM (Katona et al. 1999a).

(6) *Hilar commissural/associational path-associated (HICAP) interneurons* are characterized by an axon in the inner molecular layer, co-aligned with the commissural/associational path (Han et al. 1993; Halasy and Somogyi 1993b; Sík et al. 1997; Lübke et al. 1998; Hosp et al. 2005). The soma is located in the hilus, and the dendrites are found both in the hilus and in the molecular layer. Therefore, HICAP cells can mediate both feedforward and feedback inhibition.

(7) *Total molecular layer (TML) interneurons* project to the molecular layer, covering vertically the entire layer (Mott et al. 1997; Hosp et al. 2005). The soma is located in the cell body layer and the dendrites extend into both the hilus and the molecular layer. Therefore, TML cells can mediate inhibition to the entire dendritic tree of GCs in both feedforward and feedback manner.

Genetic Diversity of Hippocampal Interneurons

All of the neurochemical classifications of interneurons rely on differential translation of proteins, either calcium-binding, neuropeptides, transmembrane receptors and channels, or transcription factors and enzymes. All of these differentiating factors rely on differential gene expression, through DNA transcription to RNA translation. Recent advances in single-cell reverse-transcriptase PCR (RT-PCR) and RNA sequencing (RNAseq) have allowed detailed characterization of individual genetic markers and classification of inhibitory interneurons in an unbiased manner. Despite the early stage that this form of analysis is, we will highlight several genetic divergences, which partly explain interneuron diversity (Monyer and Markram 2004).

The single greatest form of genetic diversity arises from the location from which interneurons progenitors arise in the brain, the ganglionic eminences. Those neurons which are formed within the medial ganglionic eminence (mGE) are fated to become PV, NPY, and SOM. Meanwhile interneurons formed from the central ganglionic eminence (cGE) contain CCK, Reelin, and VIP. However, there is still some overlap, with nNOS and CR containing interneurons arising from both mGE and cGE (reviewed in Wamsley and Fishell 2017). These fate maps of interneuron development are underlain by precise genetic cues, with mGE expression of *Nkx2.1*, *Lhx6*, *Sox6*, and *Sip1*, the order of which defines the maturation state of these interneurons. cGE VIP neurons meanwhile selectively express *Igf1*, which controls synaptogenesis in these interneurons.

More recent adoption of single-cell RNAseq methods has allowed unbiased characterization of interneuron subtypes. For example, using this technique approximately 16 clustered subtypes of CA1 interneuron have been described (Zeisel et al. 2015). How these subtypes overlap with the 20+ described neurochemical, anatomical, and electrophysiological types remains to be seen. One technique that is approaching is the development of Patch-Seq (Fuzik et al. 2016), whereby electrophysiological recordings can be combined with RNA harvesting and anatomical tracing to determine genetic diversity. This technique, so far only applied to neocortical CCK interneurons, has identified five CCK subtypes, which is near to consistent with the number of putative cell types observed in CA1.

Experimental Techniques

Golgi Silver Staining Method

The first experimental approach that enabled detailed analysis of the morphological features of neurons was the “black reaction” developed by Camillo Golgi in the late nineteenth century. The Golgi method results in the complete labeling of a random set of neurons. The sparse staining pattern enables the examination of the

morphology of individual cells. Many neuroscientists, including Ramon y Cajal, applied this method successfully to investigate the structure and gain insights into the function of neurons in various brain areas, including the hippocampus. Although targeted labeling methods often offer clear advantages, the Golgi method can be still used to label and characterize abundant cell types (e.g., cortical principal cells). A modern version of the Golgi staining method can be observed in some transgenic lines, such as Thy1-GFP mice, in which green fluorescent protein is randomly expressed in a subset of DG GCs (Feng et al. 2000).

Immunocytochemistry

Neurons express a wide variety of molecules which can be detected and visualized using specific antibodies (Freund and Buzsáki 1996; Somogyi and Klausberger 2005; Jinno and Kosaka 2006). Some of these neurochemical markers are evenly distributed in the cytoplasm (e.g., PV, CB, and CR) or on the surface of the plasma membrane (mGluR1a); therefore, the immunostaining can delineate neurons in their entirety. Morphology of cell types with low density can be investigated using this method; however, the analysis is often restricted to the somatodendritic domain, as overlapping axonal arbors cannot be resolved with accuracy.

Targeted Labeling of Single Cells

Microelectrode and whole-cell patch-clamp recordings can be combined with intracellular labeling, using either fluorescent markers (including ion- and voltage-sensitive dyes) or biocytin/neurobiotin-based assay systems (Lacaille et al. 1987; Buhl et al. 1994a). While fluorescent dyes can be directly observed during recording, biocytin needs to be visualized by histological processing of the tissue after the recording session. This combined approach enables the identification and detailed morphological analysis of the recorded neurons to complement the physiological data. Intracellular staining of synaptically coupled neurons has been successfully used to establish the number and location of synaptic contacts. Furthermore, intracellular labeling can be combined with immunostaining to characterize the neurons neurochemically.

In vitro labeling in acute hippocampal slices has been extensively applied and provided much of the information on the structure and function of various hippocampal neurons obtained in the last two decades. However, in vitro labeling has obvious limitations in that the neurons are incomplete; part of the dendritic tree and the axon is removed during the slicing procedure. For this reason, in vivo labeling approaches, despite their lower efficiency and laborious nature, are often preferable.

In Vivo Labeling of Single Cells

In vivo labeling has been performed using microelectrode (Soltész et al. 1993; Sík et al. 1994) and more recently by whole-cell patch-clamp recordings (Lee et al. 2009). These two methods provide high-resolution electrophysiological data but inevitably lead to some degree of damage to the neurons. Alternatively, juxtacellular recordings can be performed (Klausberger et al. 2003). The physiological data, using this approach, are restricted to the discharge pattern of the neurons, but high-quality anatomical data can be obtained for correlated light and electron microscopic investigations.

The Future

Neuroanatomical investigation focusing on hippocampal neurons and networks has been performed for well over a century. These investigations have identified a large number of neuron types and provided a growing body of information on their morphology and synaptic connections. However, despite the extensive research, our knowledge is still rather limited and patchy, as this chapter also reflects.

First, classification of interneurons with atypical morphological features needs further attention. Their classification is difficult while often only one or a few examples exist in the literature. The low numbers conceivably suggest low abundance; however, the recent identification of "Ivy" interneurons (Fuentealba et al. 2008) indicates that there are still significant discoveries to be made. Second, detailed quantitative information about the morphological structure (Emri et al. 2001; Nörenberg et al. 2010) of many cell types is still missing; this would be required to create realistic single-cell models and investigate integrative properties of these neurons. Finally, connectivity of the various types should be systematically mapped (Li et al. 1992; Megías et al. 2001). While synaptic target profiles are mostly well established, divergence and convergence factors in the network have remained often unknown. This information is indispensable for our understanding of how microcircuits and large-scale networks are built and function under normal and pathological conditions.

To achieve these goals, we need to invest, no doubt, hundreds of "man-years" of dedicated and meticulous work. However, recent and future advances in experimental techniques will offer better conditions, higher efficiency, and improved resolution to morphological analysis. Novel, high-resolution imaging techniques in combination with ion- and voltage-sensitive dyes (Rózsa et al. 2004; Homma et al. 2009) and genetically encoded markers (Oliva Jr et al. 2000; Meyer et al. 2002; Livet et al. 2007) will facilitate correlated investigations of activity patterns and structure of hippocampal neurons and networks. Improved transsynaptic viral tools should advance mapping of functional and anatomical connectivity (Boldogkői et al. 2009). In combination with these methods, post hoc electron microscopic ultrastructural

investigations remain important to confirm and extend results obtained at the light microscopic level. While in vitro recording and labeling techniques continue to dominate hippocampal research, especially in the analysis of individual synaptic connections, in vivo approaches, such as juxtacellular and whole-cell patch-clamp recordings (Klausberger et al. 2003; Lee et al. 2009), will become increasingly important not only for the physiological but also for the anatomical characterization of the neurons. Wider use of these methods will help us to create large libraries of neurons and enable us on the one hand to establish general morphological features of the various neuron types and on the other to better appreciate variability of individual cells.

Further Reading

Acsády L, Arabadzisz D, Freund TF (1996a) Correlated morphological and neurochemical features identify different subsets of vasoactive intestinal polypeptide-immunoreactive interneurons in rat hippocampus. Neurosci 73:299–315

Acsády L, Görcs TJ, Freund TF (1996b) Different populations of vasoactive intestinal polypeptide-immunoreactive interneurons are specialized to control pyramidal cells or interneurons in the hippocampus. Neurosci 73:317–334

Acsády L, Kamondi A, Sík A, Freund T, Buzsáki G (1998) GABAergic cells are the major postsynaptic targets of mossy fibers in the rat hippocampus. J Neurosci 18:3386–3403

Acsády L, Katona I, Martınez-Guijarro FJ, Buzsáki G, Freund TF (2000) Unusual target selectivity of perisomatic inhibitory cells in the hilar region of the rat hippocampus. J Neurosci 20:6907–6919

Ali AB (2007) Presynaptic Inhibition of GABAA receptor-mediated unitary IPSPs by cannabinoid receptors at synapses between CCK-positive interneurons in rat hippocampus. J Neurophysiol 98:861–869

Ali AB, Thomson AM (1998) Facilitating pyramid to horizontal oriens-alveus interneurone inputs: dual intracellular recordings in slices of rat hippocampus. J Physiol 507:185–199

Amaral DG (1978) A Golgi study of cell types in the hilar region of the hippocampus in the rat. J Comp Neurol 182:851–914

Ambros-Ingerson J, Holmes WR (2005) Analysis and comparison of morphological reconstructions of hippocampal field CA1 pyramidal cells. Hippocampus 15:302–315

Armstrong C, Szabadics J, Tamás G, Soltész I (2011) Neurogliaform cells in the molecular layer of the dentate gyrus as feed-forward γ-aminobutyric acidergic modulators of entorhinal–hippocampal interplay. J Comp Neurol 519:1476–1491

Armstrong C, Krook-Magnuson E, Soltész I (2012) Neurogliaform and ivy cells: a major family of nNOS expressing GABAergic neurons. Front Neural Circuits 6(May):1–10

Bannister NJ, Larkman AU (1995a) Dendritic morphology of CA1 pyramidal neurones from the rat hippocampus: I. Branching patterns. J Comp Neurol 360:150–160

Bannister NJ, Larkman AU (1995b) Dendritic morphology of CA1 pyramidal neurones from the rat hippocampus: II. Spine distributions. J Comp Neurol 360:161–171

Bartos M, Vida I, Frotscher M, Geiger JRP, Jonas P (2001) Rapid signaling at inhibitory synapses in a dentate gyrus interneuron network. J Neurosci 21:2687–2698

Bartos M, Vida I, Frotscher M, Meyer A, Monyer H, Geiger JRP, Jonas P (2002) Fast synaptic inhibition promotes synchronized gamma oscillations in hippocampal interneuron networks. Proc Natl Acad Sci U S A 99:13222–13227

Baude A, Bleasdale C, Dalezios Y, Somogyi P, Klausberger T (2007) Immunoreactivity for the GABAA receptor alpha1 subunit, somatostatin and Connexin36 distinguishes axoaxonic, basket, and bistratified interneurons of the rat hippocampus. Cereb Cortex 17:2094–2107

Baude A, Nusser Z, Roberts JD, Mulvihill E, McIlhinney RA, Somogyi P (1993) The metabotropic glutamate receptor (mGluR1 alpha) is concentrated at perisynaptic membrane of neuronal subpopulations as detected by immunogold reaction. Neuron 11:771–787

Beining M, Jungenitz T, Radic T, Deller T, Cuntz H, Jedlicka P, Schwarzacher SW (2017) Adult-born dentate granule cells show a critical period of dendritic reorganization and are distinct from developmentally born cells. Brain Struct Funct 222:1427–1446

Bezaire MJ, Soltész I (2013) Quantitative assessment of CA1 local circuits: Knowledge base for interneuron-pyramidal cell connectivity. Hippocampus 23:751–785

Blackstad TW (1956) Commissural connections of the hippocampal region in the rat, with special reference to their mode of termination. J Comp Neurol 105:417–537

Blackstad TW, Kjaerheim A (1961) Special axo-dendritic synapses in the hippocampal cortex: electron and light microscopic studies on the layer of mossy fibers. J Comp Neurol 117:133–159

Blasco-Ibáñez JM, Freund TF (1995) Synaptic input of horizontal interneurons in stratum oriens of the hippocampal CA1 subfield: Structural basis of feed-back activation. Eur J Neurosci 7:2170–2180

Blasco-Ibáñez JM, Martínez-Guijarro F-J, Freund TF (2000) Recurrent mossy fibers preferentially innervate parvalbumin-immunoreactive interneurons in the granule cell layer of the rat dentate gyrus. Neuroreport 11:3219–3225

Bloss EB, Cembrowski MS, Karsh B, Colonell J, Fetter RD, Spruston N (2016) Structured dendritic inhibition supports branch-selective integration in CA1 pyramidal cells. Neuron 89:1016–1030

Bloss EB, Cembrowski MS, Karsh B, Colonell J, Fetter RD, Spruston N (2018) Single excitatory axons form clustered synapses onto CA1 pyramidal cell dendrites. Nature Neurosci 19:1

Boldogkői Z, Bálint K, Awatramani GB, Balya D, Busskamp V, Viney TJ, Lagali PS, Duebel J, Pásti E, Tombácz D, Tóth JS, Takács IF, Scherf BG, Roska B (2009) Genetically timed, activity-sensor and rainbow transsynaptic viral tools. Nat Methods 6:127–130

Booker SA, Gross A, Althof D, Shigemoto R, Bettler B, Frotscher M, Hearing M, Wickman K, Watanabe M, Kulik Á, Vida I (2013) Differential $GABA_B$-receptor-mediated effects in perisomatic- and dendrite-targeting parvalbumin interneurons. J Neurosci 33:7961–7974

Booker SA, Althof D, Degro CE, Watanabe M, Kulik Á, Vida I (2017a) Differential surface density and modulatory effects of presynaptic GABAB receptors in hippocampal cholecystokinin and parvalbumin basket cells. Brain Struct Funct 222:3677–3690

Booker SA, Althof D, Gross A, Loreth D, Müller J, Unger A, Fakler B, Varro A, Watanabe M, Gassmann M, Bettler B, Shigemoto R, Vida I, Kulik Á (2017b) KCTD12 auxiliary proteins modulate kinetics of GABAB receptor-mediated inhibition in cholecystokinin-containing interneurons. Cerebral Cortex (New York, N.Y.: 1991) 27:2318–2334

Booker SA, Loreth D, Gee AL, Watanabe M, Kind PC, Wyllie DJA, Kulik Á, Vida I (2018) Postsynaptic GABABRs inhibit L-type calcium channels and abolish long-term potentiation in hippocampal somatostatin interneurons. Cell Rep 22:36–43

Botcher NA, Falck JE, Thomson AM, Mercer A (2014) Distribution of interneurons in the CA2 region of the rat hippocampus. Front Neuroanatomy 8

Buckmaster PS, Strowbridge BW, Schwartzkroin PA (1993) A comparison of rat hippocampal mossy cells and CA3c pyramidal cells. J Neurophysiol 70:1281–1299

Buckmaster PS, Wenzel HJ, Kunkel DD, Schwartzkroin PA (1996) Axon arbors and synaptic connections of hippocampal mossy cells in the rat in vivo. J Comp Neurol 366:271–292

Buckmaster PS (2012) Mossy cell dendritic structure quantified and compared with other hippocampal neurons labeled in rats in vivo. Epilepsia 53(Suppl. 1):9–17

Buhl EH, Cobb SR, Halasy K, Somogyi P (1995) Properties of unitary IPSPs evoked by anatomically identified basket cells in the rat hippocampus. Eur J Neurosci 7:1989–2004

Buhl EH, Halasy K, Somogyi P (1994a) Diverse sources of hippocampal unitary inhibitory postsynaptic potentials and the number of synaptic release sites. Nature 368:823–828
Buhl EH, Han ZS, Lőrinczi Z, Stezhka VV, Karnup SV, Somogyi P (1994b) Physiological properties of anatomically identified axo-axonic cells in the rat hippocampus. J Neurophysiol 71:1289–1307
Buhl EH, Szilágyi T, Halasy K, Somogyi P (1996) Physiological properties of anatomically identified basket and bistratified cells in the CA1 area of the rat hippocampus in vitro. Hippocampus 6:294–305
Bullis JB, Jones TD, Poolos NP (2007) Reversed somatodendritic Ih gradient in a class of rat hippocampal neurons with pyramidal morphology. J Physiol 579:431–443
Cajal SR (1968) The structure of the Ammon's horn. Charles C. Thomas, Springfield
Cannon RC, Wheal HV, Turner DA (1999) Dendrites of classes of hippocampal neurons differ in structural complexity and branching patterns. J Comp Neurol 413:619–633
Carnevale NT, Tsai KY, Claiborne BJ, Brown TH (1997) Comparative electrotonic analysis of three classes of rat hippocampal neurons. J Neurophysiol 78:703–720
Cembrowski MS, Bachman JL, Wang L, Sugino K, Shields BC, Spruston N (2016a) Spatial gene-expression gradients underlie prominent heterogeneity of CA1 pyramidal neurons. Neuron 89:351–368
Cembrowski MS, Wang L, Sugino K, Shields BC, Spruston N (2016b) Hipposeq: a comprehensive RNA-seq database of gene expression in hippocampal principal neurons. eLife 5
Ceranik K, Bender R, Geiger JR, Monyer H, Jonas P, Frotscher M, Lübke J (1997) A novel type of GABAergic interneuron connecting the input and the output regions of the hippocampus. J Neurosci 17:5380–5394
Chamberland S, Salesse C, Topolnik D, Topolnik L (2010) Synapse-specific inhibitory control of hippocampal feedback inhibitory circuit. Front Cell Neurosci 4 Available at: https://www.frontiersin.org/articles/10.3389/fncel.2010.00130/full
Chevaleyre V, Siegelbaum SA (2010) Strong CA2 pyramidal neuron synapses define a powerful disynaptic cortico-hippocampal loop. Neuron 66:560–572
Chicurel ME, Harris KM (1992) Three-dimensional analysis of the structure and composition of CA3 branched dendritic spines and their synaptic relationships with mossy fiber boutons in the rat hippocampus. J Comp Neurol 325:169–182
Chitwood RA, Hubbard A, Jaffe DB (1999) Passive electrotonic properties of rat hippocampal CA3 interneurones. J Physiol 515:743–756
Christie BR, Franks KM, Seamans JK, Saga K, Sejnowski TJ (2000) Synaptic plasticity in morphologically identified CA1 stratum radiatum interneurons and giant projection cells. Hippocampus 10:673–683
Claiborne BJ, Amaral DG, Cowan WM (1986) A light and electron microscopic analysis of the mossy fibers of the rat dentate gyrus. J Comp Neurol 246:435–458
Claiborne BJ, Amaral DG, Cowan WM (1990) Quantitative, three-dimensional analysis of granule cell dendrites in the rat dentate gyrus. J Comp Neurol 302:206–219
Cobb SR, Halasy K, Vida I, Nyiri G, Tamás G, Buhl EH, Somogyi P (1997) Synaptic effects of identified interneurons innervating both interneurons and pyramidal cells in the rat hippocampus. Neurosci 79:629–648
Cope DW, Maccaferri G, Márton LF, Roberts JD, Cobden PM, Somogyi P (2002) Cholecystokinin-immunopositive basket and Schaffer collateral-associated interneurones target different domains of pyramidal cells in the CA1 area of the rat hippocampus. Neurosci 109:63–80
Csicsvari J, Hirase H, Czurkó A, Buzsáki G (1998) Reliability and state dependence of pyramidal cell-interneuron synapses in the hippocampus: An ensemble approach in the behaving rat. Neuron 21:179–189
Degro CE, Kulik A, Booker SA, Vida I (2015) Compartmental distribution of gabab receptor-mediated currents along the somatodendritic axis of hippocampal principal cells. Front Synaptic Neurosci 7(MAR):1–15
Desmond NL, Levy WB (1982) A quantitative anatomical study of the granule cell dendritic fields of the rat dentate gyrus using a novel probabilistic method. J Comp Neurol 212:131–145

Deuchars J, Thomson AM (1996) CA1 pyramid-pyramid connections in rat hippocampus in vitro: dual intracellular recordings with biocytin filling. Neuroscience 74:1009–1018

Dieni CV, Panichi R, Aimone JB, Kuo CT, Wadiche JI, Overstreet-Wadiche L (2016) Low excitatory innervation balances high intrinsic excitability of immature dentate neurons. Nat Commun 7:11313

Doischer D, Hosp JA, Yanagawa Y, Obata K, Jonas P, Vida I, Bartos M (2008) Postnatal differentiation of basket cells from slow to fast signaling devices. J Neurosci 28:12956–12968

Dong H-W, Swanson LW, Chen L, Fanselow MS, Toga AW (2009) Genomic–anatomic evidence for distinct functional domains in hippocampal field CA1. Proc Natl Acad Sci 106:11794–11799

Dougherty KA, Islam T, Johnston D (2012) Intrinsic excitability of CA1 pyramidal neurones from the rat dorsal and ventral hippocampus. J Physiol 590:5707–5722

Dougherty KA, Nicholson DA, Diaz L, Buss EW, Neuman KM, Chetkovich DM, Johnston D (2013) Differential expression of HCN subunits alters voltage-dependent gating of h-channels in CA1 pyramidal neurons from dorsal and ventral hippocampus. J Neurophysiol 109:1940–1953

Drew LJ, Kheirbek MA, Luna VM, Denny CA, Cloidt MA, Wu MV, Hen R (2016) Activation of local inhibitory circuits in the dentate gyrus by adult-born neurons. Hippocampus 26:763–778

Dumas TC, Powers EC, Tarapore PE, Sapolsky RM (2004) Overexpression of calbindin D28K in dentate gyrus granule cells alters mossy fiber presynaptic function and impairs hippocampal-dependent memory. Hippocampus 14:701–709

Elfant D, Pál BZ, Emptage N, Capogna M (2008) Specific inhibitory synapses shift the balance from feedforward to feedback inhibition of hippocampal CA1 pyramidal cells. Eur J Neurosci 27:104–113

Emri Z, Antal K, Gulyás AI, Megías M, Freund TF (2001) Electrotonic profile and passive propagation of synaptic potentials in three subpopulations of hippocampal CA1 interneurons. Neuroscience 104:1013–1026

Feng G, Mellor RH, Bernstein M, Keller-Peck C, Nguyen QT, Wallace M, Nerbonne JM, Lichtman JW, Sanes JR (2000) Imaging neuronal subsets in transgenic mice expressing multiple spectral variants of GFP. Neuron 28:41–51

Ferraguti F, Cobden P, Pollard M, Cope D, Shigemoto R, Watanabe M et al (2004) Immunolocalization of metabotropic glutamate receptor 1alpha (mGluR1alpha) in distinct classes of interneuron in the CA1 region of the rat hippocampus. Hippocampus 14:193–215

Ferraguti F, Klausberger T, Cobden P, Baude A, Roberts JD, Szucs P, Kinoshita A, Shigemoto R, Somogyi P, Dalezios Y (2005) Metabotropic glutamate receptor 8-expressing nerve terminals target subsets of GABAergic neurons in the hippocampus. J Neurosci 25:10520–10536

Földy C, Lee SH, Morgan RJ, Soltész I (2010) Regulation of fast-spiking basket cell synapses by the chloride channel ClC-2. Nature Neuroscience 13:1047–1049

Förster E, Zhao S, Frotscher M (2006) Laminating the hippocampus. Nat Rev Neurosci 7:259–267

Freund TF, Buzsáki G (1996) Interneurons of the hippocampus. Hippocampus 6:347–470

Frotscher M, Seress L, Schwerdtfeger WK, Buhl E (1991) The mossy cells of the fascia dentata: a comparative study of their fine structure and synaptic connections in rodents and primates. J Comp Neurol 312:145–163

Frotscher M, Soriano E, Misgeld U (1994) Divergence of hippocampal mossy fibers. Synapse 16:148–160

Fuentealba P, Begum R, Capogna M, Jinno S, Márton LF, Csicsvari J, Thomson A, Somogyi P, Klausberger T (2008) Ivy cells: a population of nitric-oxide-producing, slow-spiking GABAergic neurons and their involvement in hippocampal network activity. Neuron 57:917–929

Fuentealba P, Klausberger T, Karayannis T, Suen WY, Huck J, Tomioka R, Rockland K, Capogna M, Studer M, Morales M, Somogyi P (2010) Expression of COUP-TFII nuclear receptor in restricted GABAergic neuronal populations in the adult rat hippocampus. J Neurosci 30:1595–1609

Fukuda T, Kosaka T (2000) Gap junctions linking the dendritic network of GABAergic interneurons in the hippocampus. J Neurosci 20:1519–1528

Fukuda T, Kosaka T (2003) Ultrastructural study of gap junctions between dendrites of parvalbumin-containing GABAergic neurons in various neocortical areas of the adult rat. Neurosci 120:5–20

Fuzik J, Zeisel A, Mate Z, Calvigioni D, Yanagawa Y, Szabo G, Harkany T (2016) Integration of electrophysiological recordings with single-cell RNA-seq data identifies neuronal subtypes. Nat Biotechnol 34:175–183

Ganter P, Szücs P, Paulsen O, Somogyi P (2004) Properties of horizontal axo-axonic cells in stratum oriens of the hippocampal CA1 area of rats in vitro. Hippocampus 14:232–243

Geiger JR, Lübke J, Roth A, Frotscher M, Jonas P (1997) Submillisecond AMPA receptor-mediated signaling at a principal neuron-interneuron synapse. Neuron 18:1009–1023

Gloveli T, Dugladze T, Rotstein HG, Traub RD, Monyer H, Heinemann U, Whittington MA, Kopell NJ (2005a) Orthogonal arrangement of rhythm-generating microcircuits in the hippocampus. Proc Natl Acad Sci U S A 102:13295–13300

Gloveli T, Dugladze T, Saha S, Monyer H, Heinemann U, Traub RD, Whittington MA, Buhl EH (2005b) Differential involvement of oriens/pyramidale interneurones in hippocampal network oscillations in vitro. J Physiol 562:131–147

Goldin M, Epsztein J, Jorquera I, Represa A, Ben-Ari Y, Crépel V, Cossart R (2007) Synaptic Kainate Receptors Tune Oriens-Lacunosum Moleculare Interneurons to Operate at Theta Frequency. J Neurosci 27:60–9572

Golding NL, Mickus TJ, Katz Y, Kath WL, Spruston N (2005) Factors mediating powerful voltage attenuation along CA1 pyramidal neuron dendrites. J Physiol 568:69–82

Gonzales RB, DeLeon Galvan CJ, Rangel YM, Claiborne BJ (2001) Distribution of thorny excrescences on CA3 pyramidal neurons in the rat hippocampus. J Comp Neurol 430:357–368

Graves AR, Moore SJ, Bloss EB, Mensh BD, Kath WL, Spruston N (2012) Hippocampal Pyramidal Neurons Comprise Two Distinct Cell Types that Are Countermodulated by Metabotropic Receptors. Neuron 76:776–789

Guetg N, Seddik R, Vigot R, Turecek R, Gassmann M, Vogt KE, Bräuner-Osborne H, Shigemoto R, Kretz O, Frotscher M, Kulik A, Bettler B (2009) The GABAB1a isoform mediates heterosynaptic depression at hippocampal mossy fiber synapses. J Neurosci 29:1414–1423

Gulyás AI, Freund TF (1996) Pyramidal cell dendrites are the primary targets of calbindin D28k-immunoreactive interneurons in the hippocampus. Hippocampus 6:525–534

Gulyás AI, Hájos N, Freund TF (1996) Interneurons containing calretinin are specialized to control other interneurons in the rat hippocampus. J Neurosci 16:3397–3411

Gulyás AI, Megías M, Emri Z, Freund TF (1999) Total number and ratio of excitatory and inhibitory synapses converging onto single interneurons of different types in the CA1 area of the rat hippocampus. J Neurosci 19:10082–10097

Gulyás AI, Miles R, Hájos N, Freund TF (1993a) Precision and variability in postsynaptic target selection of inhibitory cells in the hippocampal CA3 region. Eur J Neurosci 5:1729–1751

Gulyás AI, Miles R, Sík A, Tóth K, Tamamaki N, Freund TF (1993b) Hippocampal pyramidal cells excite inhibitory neurons through a single release site. Nature 366:683–687

Gulyás AI, Tóth K, McBain CJ, Freund TF (1998) Stratum radiatum giant cells: a type of principal cell in the rat hippocampus. Eur J Neurosci 10:3813–3822

Gulyás AI, Hájos N, Katona I, Freund TF (2003) Interneurons are the local targets of hippocampal inhibitory cells which project to the medial septum. Eur J Neurosci 17:1861–1872

Hájos N, Acsády L, Freund TF (1996) Target selectivity and neurochemical characteristics of VIP-immunoreactive interneurons in the rat dentate gyrus. Eur J Neurosci 8:1415–1431

Hájos N, Mody I (1997) Synaptic communication among hippocampal interneurons: Properties of spontaneous IPSCs in morphologically identified cells. J Neurosci 17:8427–8442

Hájos N, Papp EC, Acsády L, Levey AI, Freund TF (1998) Distinct interneuron types express m2 muscarinic receptor immunoreactivity on their dendrites or axon terminals in the hippocampus. Neuroscience 82:355–376

Halasy K, Buhl EH, Lőrinczi Z, Tamás G, Somogyi P (1996) Synaptic target selectivity and input of GABAergic basket and bistratified interneurons in the CA1 area of the rat hippocampus. Hippocampus 6:306–329

Halasy K, Somogyi P (1993a) Distribution of GABAergic synapses and their targets in the dentate gyrus of rat: a quantitative immunoelectron microscopic analysis. J Hirnforsch 34:299–308

Halasy K, Somogyi P (1993b) Subdivisions in the multiple GABAergic innervation of granule cells in the dentate gyrus of the rat hippocampus. Eur J Neurosci 5:411–429

Hama K, Arii T, Kosaka T (1989) Three-dimensional morphometrical study of dendritic spines of the granule cell in the rat dentate gyrus with HVEM stereo images. J Electron Microsc Tech 12:80–87

Han ZS, Buhl EH, Lőrinczi Z, Somogyi P (1993) A high degree of spatial selectivity in the axonal and dendritic domains of physiologically identified local-circuit neurons in the dentate gyrus of the rat hippocampus. Eur J Neurosci 5:395–410

Harris KM, Jensen FE, Tsao B (1992) Three-dimensional structure of dendritic spines and synapses in rat hippocampus (CA1) at postnatal day 15 and adult ages: Implications for the maturation of synaptic physiology and long-term potentiation. J Neurosci 12:2685–2705

Henze DA, Cameron WE, Barrionuevo G (1996) Dendritic morphology and its effects on the amplitude and rise-time of synaptic signals in hippocampal CA3 pyramidal cells. J Comp Neurol 369:331–344

Homma R, Baker BJ, Jin L, Garaschuk O, Konnerth A, Cohen LB, Bleau CX, Canepari M, Djurisic M, Zecevic D (2009) Wide-field and two-photon imaging of brain activity with voltage- and calcium-sensitive dyes. Methods Mol Biol 489:43–79

Hooper A, Maguire J (2016) Characterization of a novel subtype of hippocampal interneurons that express corticotropin-releasing hormone. Hippocampus 26:41–53

Hormuzdi SG, Pais I, LeBeau FE, Towers SK, Rozov A, Buhl EH, Whittington MA, Monyer H (2001) Impaired electrical signaling disrupts gamma frequency oscillations in connexin 36-deficient mice. Neuron 31:487–495

Hosp JA, Strüber M, Yanagawa Y, Obata K, Vida I, Jonas P et al (2005) Morpho-physiological criteria divide dentate gyrus interneurons into classes. Hippocampus 24:189–203

Hosseini-Sharifabad M, Nyengaard JR (2007) Design-based estimation of neuronal number and individual neuronal volume in the rat hippocampus. J Neurosci Methods 162:206–214

Houser CR (2007) Interneurons of the dentate gyrus: an overview of cell types, terminal fields and neurochemical identity. Prog Brain Res 163:217–232

Igarashi KM, Ito HT, Moser EI, Moser MB (2014) Functional diversity along the transverse axis of hippocampal area CA1. FEBS Lett 588:2470–2476

Ishizuka N, Cowan WM, Amaral DG (1995) A quantitative analysis of the dendritic organization of pyramidal cells in the rat hippocampus. J Comp Neurol 362:17–45

Ishizuka N, Weber J, Amaral DG (1990) Organization of intrahippocampal projections originating from CA3 pyramidal cells in the rat. J Comp Neurol 295:580–623

Jinde S, Zsiros V, Nakazawa K (2013) Hilar mossy cell circuitry controlling dentate granule cell excitability. Front Neural Circuits 7:14

Jinno S, Klausberger T, Marton LF, Dalezios Y, Roberts JD, Fuentealba P, Bushong EA, Henze D, Buzsáki G, Somogyi P (2007) Neuronal diversity in GABAergic long-range projections from the hippocampus. J Neurosci 27:8790–8804

Jinno S, Kosaka T (2006) Cellular architecture of the mouse hippocampus: a quantitative aspect of chemically defined GABAergic neurons with stereology. Neurosci Res 56:229–245

Jouvenceau A, Potier B, Battini R, Ferrari S, Dutar P, Billard JM (1999) Glutamatergic synaptic responses and long-term potentiation are impaired in the CA1 hippocampal area of calbindin D(28K)-deficient mice. Synapse 33:172–180

Karson MA, Tang AH, Milner TA, Alger BE (2009) Synaptic cross talk between perisomatic-targeting interneuron classes expressing cholecystokinin and parvalbumin in hippocampus. J Neurosci 29:4140–4154

Katona I, Acsády L, Freund TF (1999a) Postsynaptic targets of somatostatin-immunoreactive interneurons in the rat hippocampus. Neuroscience 88:37–55

Katona I, Sperlágh B, Sík A, Käfalvi A, Vizi ES, Mackie K, Freund TF (1999b) Presynaptically located CB1 cannabinoid receptors regulate GABA release from axon terminals of specific hippocampal interneurons. J Neurosci 19:4544–4558

Katona L, Micklem B, Borhegyi Z, Swiejkowski DA, Valenti O, Viney TJ, Kotzadimitriou D, Klausberger T, Somogyi P (2017) Behavior-dependent activity patterns of GABAergic long-range projecting neurons in the rat hippocampus. Hippocampus 27:359–377

Katsumaru H, Kosaka T, Heizmann CW, Hama K (1988) Immunocytochemical study of GABAergic neurons containing the calcium-binding protein parvalbumin in the rat hippocampus. Exp Brain Res 72:347–362

Kempermann G, Jessberger S, Steiner B, Kronenberg G (2004) Milestones of neuronal development in the adult hippocampus. Trends Neurosci 27:447–452

Kepecs A, Fishell G (2014) Interneuron cell types are fit to function. Nature 505:318–326

Klausberger T, Magill PJ, Márton LF, Roberts JD, Cobden PM, Buzsáki G, Somogyi P (2003) Brain-state- and cell-type-specific firing of hippocampal interneurons in vivo. Nature 421:844–848

Klausberger T, Márton LF, Baude A, Roberts JD, Magill PJ, Somogyi P (2004) Spike timing of dendrite-targeting bistratified cells during hippocampal network oscillations in vivo. Nat Neurosci 7:41–47

Klausberger T, Marton LF, O'Neill J, Huck JH, Dalezios Y, Fuentealba P, Suen WY, Papp E, Kaneko T, Watanabe M, Csicsvari J, Somogyi P (2005) Complementary roles of cholecystokinin- and parvalbumin-expressing GABAergic neurons in hippocampal network oscillations. J Neurosci 25:9782–9793

Klausberger T, Somogyi P (2008) Neuronal diversity and temporal dynamics: the unity of hippocampal circuit operations. Science 321:53–57

Klausberger T (2009) GABAergic interneurons targeting dendrites of pyramidal cells in the CA1 area of the hippocampus. Eur J Neurosci 30:947–957

Kohara K, Pignatelli M, Rivest AJ, Jung HY, Kitamura T, Suh J, Frank D, Kajikawa K, Mise N, Obata Y, Wickersham IR, Tonegawa S (2014) Cell type-specific genetic and optogenetic tools reveal hippocampal CA2 circuits. Nat Neurosci 17:269–279

Kosaka T (1980) The axon initial segment as a synaptic site: Ultrastructure and synaptology of the initial segment of the pyramidal cell in the rat hippocampus (CA3 region). J Neurocytol 9:861–882

Kosaka T, Katsumaru H, Hama K, Wu JY, Heizmann CW (1987) GABAergic neurons containing the Ca^{2+}-binding protein parvalbumin in the rat hippocampus and dentate gyrus. Brain Res 419:119–130

Kosaka T, Wu JY, Benoit R (1988) GABAergic neurons containing somatostatin-like immunoreactivity in the rat hippocampus and dentate gyrus. Exp Brain Res 71:388–398

Kowalski J, Geuting M, Paul S, Dieni S, Laurens J, Zhao S, Drakew A, Haas CA, Frotscher M, Vida I (2010) Proper layering is important for precisely timed activation of hippocampal mossy cells. Cereb Cortex 20:2043–2054

Kraushaar U, Jonas P (2000) Efficacy and stability of quantal GABA release at a hippocampal interneuron-principal neuron synapse. J Neurosci 20:5594–5607

Krook-Magnuson E, Luu L, Lee S-H, Varga C, Soltész I (2011) Ivy and neurogliaform interneurons are a major target of μ-opioid receptor modulation. J Neurosci 31:14861–14870

Lacaille JC, Mueller AL, Kunkel DD, Schwartzkroin PA (1987) Local circuit interactions between oriens/alveus interneurons and CA1 pyramidal cells in hippocampal slices: electrophysiology and morphology. J Neurosci 7:1979–1993

Larimer P, Strowbridge BW (2008) Non-random local circuits in the dentate gyrus. J Neurosci 28:12212–12223

Leão RN, Mikulovic S, Leão KE, Munguba H, Gezelius H, Enjin A, Patra K, Eriksson A, Loew LM, Tort ABL, Kullander K (2012) OLM interneurons differentially modulate CA3 and entorhinal inputs to hippocampal CA1 neurons. Nat Neurosci 15:1524–1530

Lee AK, Epsztein J, Brecht M (2009) Head-anchored whole-cell recordings in freely moving rats. Nat Protoc 4:385–392

Lee SE, Simons SB, Heldt SA, Zhao M, Schroeder JP, Vellano CP, Cowan DP, Ramineni S, Yates CK, Feng Y, Smith Y, Sweatt JD, Weinshenker D, Ressler KJ, Dudek SM, Hepler JR (2010) RGS14 is a natural suppressor of both synaptic plasticity in CA2 neurons and hippocampal-based learning and memory. Proc Natl Acad Sci U S A 107:16994–16998

Lee SH, Marchionni I, Bezaire M, Varga C, Danielson N, Lovett-Barron M, Losonczy A, Soltész I (2014) Parvalbumin-positive basket cells differentiate among hippocampal pyramidal cells. Neuron 82:1129–1144

Lein ES, Callaway EM, Albright TD, Gage FH (2005) Redefining the boundaries of the hippocampal CA2 subfield in the mouse using gene expression and 3-dimensional reconstruction. J Comp Neurol 485:1–10

Li XG, Somogyi P, Tepper JM, Buzsáki G (1992) Axonal and dendritic arborization of an intracellularly labeled chandelier cell in the CA1 region of rat hippocampus. Exp Brain Res 90:519–525

Li XG, Somogyi P, Ylinen A, Buzsáki G (1994) The hippocampal CA3 network: an in vivo intracellular labeling study. J Comp Neurol 339:181–208

Livet J, Weissman TA, Kang H, Draft RW, Lu J, Bennis RA, Sanes JR, Lichtman JW (2007) Transgenic strategies for combinatorial expression of fluorescent proteins in the nervous system. Nature 450:56–62

Lorente de Nó R (1934) Studies on the structure of the cerebral cortex II: Continuation of the study of the ammonic system. J Psychol Neurol 46:113–177

Losonczy A, Biró AA, Nusser Z (2004) Persistently active cannabinoid receptors mute a subpopulation of hippocampal interneurons. Proc Natl Acad Sci U S A 101:1362–1367

Luuk H, Koks S, Plaas M, Hannibal J, Rehfeld JF, Vasar E (2008) Distribution of Wfs1 protein in the central nervous system of the mouse and its relation to clinical symptoms of the Wolfram syndrome. J Comp Neurol 509:642–660

Lübke J, Frotscher M, Spruston N (1998) Specialized electrophysiological properties of anatomically identified neurons in the hilar region of the rat fascia dentata. J Neurophysiol 79:1518–1534

Maccaferri G, Dingledine R (2002) Control of feedforward dendritic inhibition by NMDA receptor-dependent spike timing in hippocampal interneurons. J Neurosci 22:5462–5472

Maccaferri G, Lacaille JC (2003) Interneuron diversity series: Hippocampal interneuron classifications – making things as simple as possible, not simpler. Trends Neurosci 26:564–571

Maccaferri G, Roberts JD, Szucs P, Cottingham CA, Somogyi P (2000) Cell surface domain specific postsynaptic currents evoked by identified GABAergic neurones in rat hippocampus in vitro. J Physiol 524:91–116

Maglóczky Z, Acsády L, Freund TF (1994) Principal cells are the postsynaptic targets of supramammillary afferents in the hippocampus of the rat. Hippocampus 4:322–334

Major G, Evans JD, Jack JJB (1993) Solutions for transients in arbitrarily branching cables: 1. Voltage recording with a somatic shunt. Biophys J 65:423–449

Major G, Larkman AU, Jonas P, Sakmann B, Jack JJ (1994) Detailed passive cable models of whole-cell recorded CA3 pyramidal neurons in rat hippocampal slices. J Neurosci 14:4613–4638

Masurkar AV, Srinivas KV, Brann DH, Warren R, Lowes DC, Siegelbaum SA (2017) Medial and lateral entorhinal cortex differentially excite deep versus superficial CA1 pyramidal neurons. Cell Rep 18:148–160

Martina M, Vida I, Jonas P (2000) Distal initiation and active propagation of action potentials in interneuron dendrites. Science 287:295–300

Mátyás F, Freund TF, Gulyás AI (2004) Convergence of excitatory and inhibitory inputs onto CCK-containing basket cells in the CA1 area of the rat hippocampus. Eur J Neurosci 19:1243–1256

McBain CJ, DiChiara TJ, Kauer JA (1994) Activation of metabotropic glutamate receptors differentially affects two classes of hippocampal interneurons and potentiates excitatory synaptic transmission. J Neurosci 14:4433–4445

McBain CJ, Fisahn A (2001) Interneurons unbound. Nat Rev Neurosci 2:11–23

Megías M, Emri Z, Freund TF, Gulyás AI (2001) Total number and distribution of inhibitory and excitatory synapses on hippocampal CA1 pyramidal cells. Neurosci 102:527–540

Melzer S, Michael M, Caputi A, Eliava M, Fuchs EC, Whittington MA, Monyer H (2012) Long-range-projecting gabaergic neurons modulate inhibition in hippocampus and entorhinal cortex. Science 335:1506–1510

Mercer A, Trigg HL, Thomson AM (2007) Characterization of neurons in the CA2 subfield of the adult rat hippocampus. J Neurosci 27:7329–7338

Meyer AH, Katona I, Blatow M, Rozov A, Monyer H (2002) In vivo labeling of parvalbumin-positive interneurons and analysis of electrical coupling in identified neurons. J Neurosci 22:7055–7064

Miettinen R, Hajszan T, Riedel A, Szigeti-Buck K, Leranth C (2012) Estimation of the total number of hippocampal CA1 pyramidal neurons: New methodology applied to helpless rats. J Neurosci Methods 205:130–138

Mikulovic S, Restrepo CE, Hilscher MM, Kullander K, Leão RN (2015) Novel markers for OLM interneurons in the hippocampus. Front Cell Neurosci 9:201

Miles R, Tóth K, Gulyás AI, Hájos N, Freund TF (1996) Differences between somatic and dendritic inhibition in the hippocampus. Neuron 16:815–823

Milior G, Di Castro MA, Sciarria LP, Garofalo S, Branchi I, Ragozzino D, Limatola C, Maggi L (2016) Electrophysiological properties of CA1 pyramidal neurons along the longitudinal axis of the mouse hippocampus. Scientific Rep 6:38242

Min MY, Melyan Z, Kullmann DM (1999) Synaptically released glutamate reduces gamma-aminobutyric acid GABAergic inhibition in the hippocampus via kainite receptors. Proc Natl Acad Sci U S A 96:9932–9937

Mizuseki K, Diba K, Pastalkova E, Buzsáki G (2011) Hippocampal CA1 pyramidal cells form functionally distinct sublayers. Nat Neurosci 14:1174–1181

Monyer H, Markram H (2004) Interneuron Diversity series: Molecular and genetic tools to study GABAergic interneuron diversity and function. Trends Neurosci 27:90–97

Mott DD, Turner DA, Okazaki MM, Lewis DV (1997) Interneurons of the dentate-hilus border of the rat dentate gyrus: morphological and electrophysiological heterogeneity. J Neurosci 17:3990–4005

Nörenberg A, Hu H, Vida I, Bartos M, Jonas P (2010) Distinct nonuniform cable properties optimize rapid and efficient activation of fast-spiking GABAergic interneurons. PNAS 107:894–899

Nunzi MG, Gorio A, Milan F, Freund TF, Somogyi P, Smith AD (1985) Cholecystokinin-immunoreactive cells form symmetrical synaptic contacts with pyramidal and nonpyramidal neurons in the hippocampus. J Comp Neurol 237:485–505

Oláh S, Füle M, Komlósi G, Varga C, Báldi R, Barzó P, Tamás G (2009) Regulation of cortical microcircuits by unitary GABA-mediated volume transmission. Nature 461:1278–1281

Oliva AA Jr, Jiang M, Lam T, Smith KL, Swann JW (2000) Novel hippocampal interneuronal subtypes identified using transgenic mice that express green fluorescent protein in GABAergic interneurons. J Neurosci 20:3354–3368

Palmer LM, Stuart GJ (2006) Site of action potential initiation in layer 5 pyramidal neurons. J Neurosci 26:1854–1863

Pawelzik H, Hughes DI, Thomson AM (2002) Physiological and morphological diversity of immunocytochemically defined parvalbumin- and cholecystokinin-positive interneurones in CA1 of the adult rat hippocampus. J Comp Neurol 443:346–367

Pelkey KA, Chittajallu R, Craig MT, Tricoire L, Wester JC, McBain CJ (2017) Hippocampal GABAergic inhibitory interneurons. Physiol Rev 97:1619–1747

Petilla Interneuron Nomenclature Group, Ascoli GA, Alonso-Nanclares L, Anderson SA, Barrionuevo G, Benavides-Piccione R, Burkhalter A, Buzsáki G, Cauli B, Defelipe J, Fairén A, Feldmeyer D, Fishell G, Fregnac Y, Freund TF, Gardner D, Gardner EP, Goldberg JH, Helmstaedter M, Hestrin S, Karube F, Kisvárday ZF, Lambolez B, Lewis DA, Marin O, Markram H, Munoz A, Packer A, Petersen CC, Rockland KS, Rossier J, Rudy B, Somogyi P, Staiger JF, Tamas G, Thomson AM, Toledo-Rodriguez M, Wang Y, West DC, Yuste R (2008)

Petilla terminology: nomenclature of features of GABAergic interneurons of the cerebral cortex. Nat Rev Neurosci 9:557–568
Price CJ, Cauli B, Kovacs ER, Kulik A, Lambolez B, Shigemoto R, Capogna M (2005) Neurogliaform neurons form a novel inhibitory network in the hippocampal CA1 area. J Neurosci 25:6775–6786
Price CJ, Scott R, Rusakov DA, Capogna M (2008) GABA(B) receptor modulation of feedforward inhibition through hippocampal neurogliaform cells. J Neurosci 28:6974–6982
Pyapali GK, Sík A, Penttonen M, Buzsáki G, Turner DA (1998) Dendritic properties of hippocampal CA1 pyramidal neurons in the rat: Intracellular staining in vivo and in vitro. J Comp Neurol 391:335–352
Ratzliff AH, Santhakumar V, Howard A, Soltész I (2002) Mossy cells in epilepsy: Rigor mortis or vigor mortis? Trends Neurosci 25:140–144
Ribak CE, Seress L, Amaral DG (1985) The development, ultrastructure and synaptic connections of the mossy cells of the dentate gyrus. J Neurocytol 14:835–857
Rollenhagen A, Sätzler K, Rodríguez EP, Jonas P, Frotscher M, Lübke JH (2007) Structural determinants of transmission at large hippocampal mossy fiber synapses. J Neurosci 27:10434–10444
Rózsa B, Zelles T, Vizi ES, Lendvai B (2004) Distance-dependent scaling of calcium transients evoked by backpropagating spikes and synaptic activity in dendrites of hippocampal interneurons. J Neurosci 24:661–670
Ruchi M, Ann DK, Komal P, Connor B, Daniel J (2016) Mapping the electrophysiological and morphological properties of CA1 pyramidal neurons along the longitudinal hippocampal axis. Hippocampus 26:341–361
Scharfman HE (1991) Dentate hilar cells with dendrites in the molecular layer have lower thresholds for synaptic activation by perforant path than granule cells. J Neurosci 11:1660–1673
Scharfman HE (1994) Evidence from simultaneous intracellular recordings in rat hippocampal slices that area CA3 pyramidal cells innervate dentate hilar mossy cells. J Neurophysiol 72:2167–2180
Scharfman HE (1995) Electrophysiological diversity of pyramidal-shaped neurons at the granule cell layer/hilus border of the rat dentate gyrus recorded in vitro. Hippocampus 5:287–305
Scharfman HE (2007) The CA3 “backprojection” to the dentate gyrus. Prog Brain Res 163: 627–637
Scharfman HE (2016) The enigmatic mossy cell of the dentate gyrus. Nat Rev Neurosci 17: 562–575
Schmidt-Hieber C, Jonas P, Bischofberger J (2007) Subthreshold dendritic signal processing and coincidence detection in dentate gyrus granule cells. J Neurosci 27:8430–8441
Seress L, Pokorny J (1981) Structure of the granular layer of the rat dentate gyrus. A light microscopic and Golgi study. J Anat 133:181–195
Seri B, García-Verdugo JM, Collado-Morente L, McEwen BS, Alvarez-Buylla A (2004) Cell types, lineage, and architecture of the germinal zone in the adult dentate gyrus. J Comp Neurol 478:359–378
Sík A, Penttonen M, Buzsáki G (1997) Interneurons in the hippocampal dentate gyrus: an in vivo intracellular study. Eur J Neurosci 9:573–588
Sík A, Penttonen M, Ylinen A, Buzsáki G (1995) Hippocampal CA1 interneurons: an in vivo intracellular labeling study. J Neurosci 15:6651–6665
Sík A, Tamamaki N, Freund TF (1993) Complete axon arborization of a single CA3 pyramidal cell in the rat hippocampus, and its relationship with postsynaptic parvalbumin-containing interneurons. Eur J Neurosci 5:1719–1728
Sík A, Ylinen A, Penttonen M, Buzsáki G (1994) Inhibitory CA1–CA3-hilar region feedback in the hippocampus. Science. 265:1722–1724
Slomianka L, Amrein I, Knuesel I, Sørensen JC, Wolfer DP (2011) Hippocampal pyramidal cells: The reemergence of cortical lamination. Brain Struct Funct 216:301–317

Sloviter RS (1989) Calcium-binding protein (calbindin-D28k) and parvalbumin immunocytochemistry: localization in the rat hippocampus with specific reference to the selective vulnerability of hippocampal neurons to seizure activity. J Comp Neurol 280:183–196

Sloviter RS, Zappone CA, Harvey BD, Bumanglag AV, Bender RA, Frotscher M (2003) "Dormant basket cell" hypothesis revisited: relative vulnerabilities of dentate gyrus mossy cells and inhibitory interneurons after hippocampal status epilepticus in the rat. J Comp Neurol 459: 44–76

Soltész I, Bourassa J, Desche^nes M (1993) The behavior of mossy cells of the rat dentate gyrus during theta oscillations in vivo. Neurosci 57:555–564

Somogyi P, Dalezios Y, Lujan R, Roberts JD, Watanabe M, Shigemoto R (2003) High level of mGluR7 in the presynaptic active zones of select populations of GABAergic terminals innervating interneurons in the rat hippocampus. Eur J Neurosci 17:2503–2520

Somogyi J, Baude A, Omori Y, Shimizu H, El Mestikawy S, Fukaya M, Shigemoto R, Watanabe M, Somogyi P (2004) GABAergic basket cells expressing cholecystokinin contain vesicular glutamate transporter type 3 (VGLUT3) in their synaptic terminals in hippocampus and isocortex of the rat. Eur J Neurosci 19:552–569

Somogyi P, Klausberger T (2005) Defined types of cortical interneurone structure space and spike timing in the hippocampus. J Physiol 562:9–26

Somogyi P, Nunzi MG, Gorio A, Smith AD (1983) A new type of specific interneuron in the monkey hippocampus forming synapses exclusively with the axon initial segments of pyramidal cells. Brain Res 259:137–142

Srinivas KV, Buss EW, Sun Q, Santoro B, Takahashi H, Nicholson DA, Siegelbaum SA (2017) The dendrites of CA2 and CA1 pyramidal neurons differentially regulate information flow in the cortico-hippocampal circuit. J Neurosci 37(12):3276–3293

Stafford MM, Brown MN, Mishra P, Stanwood GD, Mathews GC (2009) Glutamate spillover augments GABA synthesis and release from axodendritic synapses in rat hippocampus. Hippocampus 20:134–144

Stuart GJ, Sakmann B (1994) Active propagation of somatic action potentials into neocortical pyramidal cell dendrites. Nature 367:69–72

Szabadics J, Tamás G, Soltész I (2007) Different transmitter transients underlie presynaptic cell type specificity of GABAA,slow and GABAA,fast. Proc Natl Acad Sci U S A 104:14831–14836

Takács VT, Klausberger T, Somogyi P, Freund TF, Gulyás AI (2012) Extrinsic and local glutamatergic inputs of the rat hippocampal CA1 area differentially innervate pyramidal cells and interneurons. Hippocampus 22:1379–1391

Tamamaki N, Abe K, Nojyo Y (1988) Three-dimensional analysis of the whole axonal arbors originating from single CA2 pyramidal neurons in the rat hippocampus with the aid of a computer graphic technique. Brain Res 452:255–272

Tamás G, Lőrincz A, Simon A, Szabadics J (2003) Identified sources and targets of slow inhibition in the neocortex. Science 299:1902–1905

Thome C, Kelly T, Yanez A, Schultz C, Engelhardt M, Cambridge SB, Egorov AV (2014) Axon-carrying dendrites convey privileged synaptic input in hippocampal neurons. Neuron 83: 1418–1430

Thompson CL, Pathak SD, Jeromin A, Ng LL, MacPherson CR, Mortrud MT, Cusick A, Riley ZL, Sunkin SM, Bernard A, Puchalski RB, Gage FH, Jones AR, Bajic VB, Hawrylycz MJ, Lein ES (2008) Genomic anatomy of the hippocampus. Neuron 60:1010–1021

Thurbon D, Field A, Redman S (1994) Electrotonic profiles of interneurons in stratum pyramidale of the CA1 region of rat hippocampus. J Neurophysiol 71:1948–1958

Tóth K, McBain CJ (1998) Afferent-specific innervation of two distinct AMPA receptor subtypes on single hippocampal interneurons. Nat Neurosci 1:572–578

Tricoire L, Pelkey KA, Daw MI, Sousa VH, Miyoshi G, Jeffries B, McBain CJ (2010) Common origins of hippocampal ivy and nitric oxide synthase expressing neurogliaform cells. J Neurosci 30:2165–2176

Traub RD, Jefferys JG, Miles R, Whittington MA, Tóth K (1994) A branching dendritic model of a rodent CA3 pyramidal neurone. J Physiol 481:79–95

Turner DA, Li XG, Pyapali GK, Ylinen A, Buzsáki G (1995) Morphometric and electrical properties of reconstructed hippocampal CA3 neurons recorded in vivo. J Comp Neurol 356:580–594

Tyan L, Chamberland S, Magnin E, Camire O, Francavilla R, David LS, Topolnik L (2014) Dendritic inhibition provided by interneuron-specific cells controls the firing rate and timing of the hippocampal feedback inhibitory circuitry. J Neurosci 34:4534–4547

Urban-Ciecko J, Fanselow EE, Barth AL (2015) Neocortical somatostatin neurons reversibly silence excitatory transmission via GABAb receptors. Curr Biol 25:722–731

Yan X-X, Toth Z, Schultz L, Ribak CE, Baram TZ (1998) Corticotropin-Releasing Hormone (CRH)-containing neurons in the immature rat hippocampal formation: light and electron microscopic features and colocalization with glutamate decarboxylase and parvalbumin. Hippocampus 8:231–243

Vida I, Frotscher M (2000) A hippocampal interneuron associated with the mossy fiber system. Proc Natl Acad Sci U S A 97:1275–1280

Vida I, Halasy K, Szinyei C, Somogyi P, Buhl EH (1998) Unitary IPSPs evoked by interneurons at the stratum radiatum-stratum lacunosum-moleculare border in the CA1 area of the rat hippocampus in vitro. J Physiol 506:755–773

Vivar C, Potter MC, Choi J, Lee JY, Stringer TP, Callaway EM, Gage FH, Suh H, Van Praag H (2012) Monosynaptic inputs to new neurons in the dentate gyrus. Nat Commun 3

Vogt KE, Nicoll RA (1999) Glutamate and gamma-aminobutyric acid mediate a heterosynaptic depression at mossy fiber synapses in the hippocampus. Proc Natl Acad Sci U S A 96:1118–1122

Vuksic M, Del Turco D, Bas Orth C, Burbach GJ, Feng G, Müller CM, Schwarzacher SW, Deller T (2008) 3D-reconstruction and functional properties of GFP-positive and GFP-negative granule cells in the fascia dentata of the Thy1-GFP mouse. Hippocampus 18:364–375

Wamsley B, Fishell G (2017) Genetic and activity-dependent mechanisms underlying interneuron diversity. Nat Rev Neurosci 18:299–309

Williams PA, Larimer P, Gao Y, Strowbridge BW (2007) Semilunar granule cells: glutamatergic neurons in the rat dentate gyrus with axon collaterals in the inner molecular layer. J Neurosci 27:13756–13761

Wittner L, Henze DA, Záborszky L, Buzsáki G (2006) Hippocampal CA3 pyramidal cells selectively innervate aspiny interneurons. Eur J Neurosci 24:1286–1298

Wittner L, Henze DA, Záborszky L, Buzsáki G (2007) Three-dimensional reconstruction of the axon arbor of a CA3 pyramidal cell recorded and filled in vivo. Brain Struct Funct 212:75–83

Zeisel A, Manchado ABM, Codeluppi S, Lonnerberg P, La Manno G, Jureus A, Linnarsson S (2015) Cell types in the mouse cortex and hippocampus revealed by single-cell RNA-seq. Science 347:1138–1142

Zhao C (2006) Distinct morphological stages of dentate granule neuron maturation in the adult mouse hippocampus. J Neurosci 26:3–11